Bulletin of the Mineral Research and Exploration

http://bulletin.mta.gov.tr

Mineral chemistry, petrography and crystallization conditions of the Middle Eocene Kazıkbeli Pluton (Eastern Pontides, NE Türkiye)

Zikrullah Samet GÜLOĞLU[a*], Abdullah KAYGUSUZ[b], Emre AYDINÇAKIR[b] and Cem YÜCEL[c]

[a] *Zonguldak Bülent Ecevit University, Department of Mining and Mineral Extraction, Zonguldak, Türkiye*
[b] *Gümüşhane University, Department of Geological Engineering, Gümüşhane, Türkiye*
[c] *Gümüşhane University, Department of Mining Engineering, Gümüşhane, Türkiye*

Research Article

Keywords:
Petrography,
Mineral Chemistry,
Geothermobarometer,
Kürtün (NE Türkiye),
Eastern Pontides.

ABSTRACT

The Eastern Pontides host a diverse suite of plutonic rocks spanning a wide range of ages and compositions. Among these, the Middle Eocene Kazıkbeli pluton, located in the Kürtün district of Gümüşhane, stands out due to its distinctive petrological characteristics. This study aims to unravel the petrological implications of petrographic and mineral chemical data to determine the physicochemical conditions (temperature, pressure, oxygen fugacity) under which the Kazıkbeli magma crystallized and was emplaced. By integrating mineral chemical data, we seek to quantify emplacement pressure, crystallization temperature, and oxygen fugacity. A comprehensive understanding of the genetic relationships and physicochemical properties of the Kazıkbeli pluton rocks, as determined through geological, petrographic and mineral chemistry, is crucial for elucidating the geological evolution of the Eastern Pontides. The Kazıkbeli Pluton exhibits a predominant NE-SW orientation and encompasses an area of roughly 46 km². Modal mineralogical analysis reveals a compositional spectrum ranging from gabbroic diorite to monzogranite, with granodiorite and tonalite being the most prominent rock types. Textural variations encompass fine- to medium-grained, porphyritic, poikilitic, and occasionally graphic textures. The primary mineral assemblage of the pluton comprises plagioclase, orthoclase, quartz, amphibole, biotite, and Fe-Ti oxides. Accessory minerals include zircon, apatite, sphene, and allanite. Plagioclases are labradorite to oligoclase (An_{26} to An_{66}) in composition. K-feldspar minerals exhibited an orthoclase composition (Or_{80} to Or_{97}). All amphiboles belong to the calcic amphibole field and exhibit a magnesio-hornblende (Mg#=0.63-0.73) composition. Biotites crystallized as solidified melt products with compositions between annite and phlogopite endmembers, plotting close to the magnesium-rich (Mg#=0.52-0.58) end of the phlogopite solid solution series. Calculated crystallization temperatures derived from amphibole and biotite data range from 712°C to 824°C. Pressure estimations calculated using amphibole-plagioclase, amphibole and biotite suggest a range of 0.04 to 2.06 kbar. Oxygen fugacity (fO_2) values calculated using amphibole and biotite fall between -12.5 and -16.1. Amphibole-based water content estimations indicate a range of 3.7% to 5.7% for the pluton. Biotite compositions within the studied Kazıkbeli pluton rocks exhibit characteristics suggestive of a potential mantle origin. Geobarometric calculations based on mineral chemistry data with geological and petrographic features indicate the emplacement of the Kazıkbeli Pluton at relatively shallow depths within the crust (~1 to 8 km).

Received Date: 26.01.2024
Accepted Date: 07.08.2024

Citation Info: Güloğlu, Z. S., Kaygusuz, A., Aydınçakır, E., Yüzel, C. 2024. Mineral chemistry, petrography and crystallization conditions of the Middle Eocene Kazıkbeli Pluton (Eastern Pontides, NE Turkey). Bulletin of the Mineral Research and Exploration 175, 83-109. https://doi.org/10.19111/bulletinofmre.1529525

**Corresponding author: Zikrullah Samet GÜLOĞLU, sametguloglu610@gmail.com*

1. Introduction

The Eastern Pontides Orogenic Belt (EPOB) constitutes a critical area for examining plutonic and volcanic lithologies (Okay and Şahintürk, 1997; Kaygusuz and Şahin, 2016; Özdamar, 2016; Temizel et al., 2019; Gücer and Sarı, 2021; Arslan et al., 2022; Kaygusuz et al., 2022, 2023; Oğuz-Saka et al., 2023; Sar et al., 2023; Revan et al., 2023; Rezeau et al., 2023). The EPOB exhibits a rich tapestry of plutonic bodies, with emplacement ages spanning from the Carboniferous to the Eocene (Figure 1). Notably, these plutons display a compositional spectrum ranging from gabbro to granite (Figure 1). Further analysis reveals four distinct intrusive episodes within the EPOB: Paleozoic (Carboniferous), Jurassic, Late Cretaceous, and Eocene (Figure 1). Paleozoic plutons were intruded into metamorphic rocks (Yılmaz, 1972; Çoğulu, 1975; Topuz et al., 2010; Dokuz, 2011; Kaygusuz et al., 2012, 2016; Ustaömer et al., 2013; Gücer and Sarı, 2021), Jurassic plutons were emplaced into pre-Jurassic basement rocks (Eyüboğlu et al., 2016; Karslı et al., 2017; Dokuz and Sünnetçi, 2019; Aydınçakır et al., 2020, 2023), Late Cretaceous plutons cut across subduction-related volcanic and/or volcaniclastic rocks (Kaygusuz, 2000; Boztuğ et al., 2006; İlbeyli, 2008; Kaygusuz et al., 2008, 2021; Liu et al., 2018; Eyüboğlu et al., 2019; Temizel et al., 2019, 2022; Yücel et al., 2023), and Eocene plutons intrude all previous units (Topuz et al., 2005, 2011; Karslı et al., 2007, 2011; Kaygusuz and Öztürk, 2015; Eyüboğlu et al., 2017, 2018; Kaygusuz et al., 2017, 2018, 2020; Özdamar et al., 2017; Sipahi et al., 2017; Temizel et al., 2018, 2020; Vural and Kaygusuz, 2021; Aydınçakır et al., 2022).

The chemical composition and evolution of the melt, as reflected by the mineral assemblage and the geochemical signature of the constituent minerals, are intrinsically linked in igneous rocks (Abbott, 1985). Variations in temperature (T), pressure (P), and oxygen fugacity (fO_2) are recognized as the principal factors controlling mineral formation and stability within magma. Determining these intensive variables (T, P, fO_2) offers valuable insights into the crystallization processes that govern magma evolution. Thermodynamic principles allow us to predict the mineralogical assemblage that crystallizes under specific conditions. While previous studies have addressed the emplacement conditions of some Eastern Pontide plutons (e.g., Karslı et al., 2007; Eyüboğlu et al., 2017; Kaygusuz et al., 2018, 2020; Temizel et al., 2018; Aydınçakır et al., 2020), the Kazıkbeli pluton remained unexamined in this context. This investigation, therefore, presents the first attempt to elucidate the pressure-temperature history of the Kazıkbeli pluton, offering new construction on its crystallization environment.

Prior investigations of the Kazıkbeli Pluton have been defined by broad geological surveys

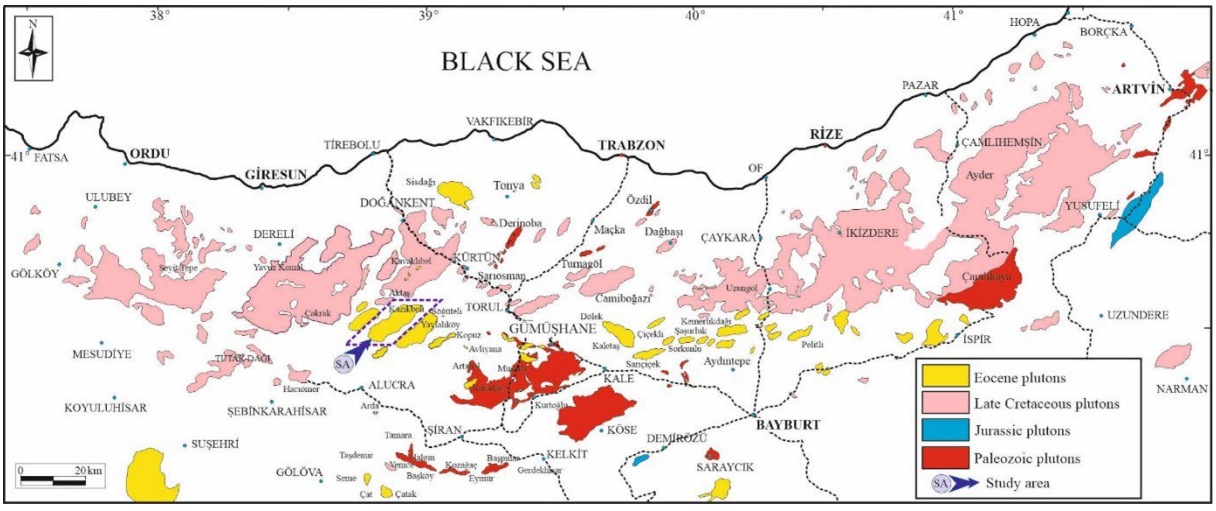

Figure 1- The location of the studied Kazıkbeli Pluton and the established distribution of plutonic rocks within the Eastern Pontides (modified after Güven, 1993 and Güloğlu, 2022).

(Güven, 1993). In-depth analyses were only recently undertaken by the lead author of this paper as part of their doctoral dissertation (Güloğlu, 2022). The present study delves into a specific aspect of Güloğlu's (2022) comprehensive doctoral research.

This investigation focuses on the petrographic and mineral chemical characteristics of the Middle Eocene Kazıkbeli Pluton exposed within the Kürtün region, Gümüşhane Province (Figure 2). By employing mineral chemistry data, the study aims to decipher the thermobarometric conditions (pressure-temperature) that prevailed during the pluton's crystallization. The findings will contribute to the existing body of knowledge regarding the emplacement conditions of the pluton.

2. Geological Position and Field Characteristics of the Kazıkbeli Pluton

The geologic record within the study area unveils a sequence of sedimentary and volcanic units (Figure 2). The oldest exposed unit is the Liassic-Doggerian aged Hamurkesen Formation (Ağar, 1977), composed primarily of basaltic and andesitic lavas with minor pyroclastics. Outcrops of this formation are limited to a small area north of the study region. Conformably overlying the Hamurkesen Formation is the widespread Late Cretaceous aged Çatak Formation (Güven, 1993). This formation dominates the study area and is characterized by andesites at lower levels, transitioning upwards to tuff-dominated sequences with minor andesites and intercalations of limestones and tuffites. The Late Cretaceous stratigraphy continues with the Kızılkaya Formation (Güven,

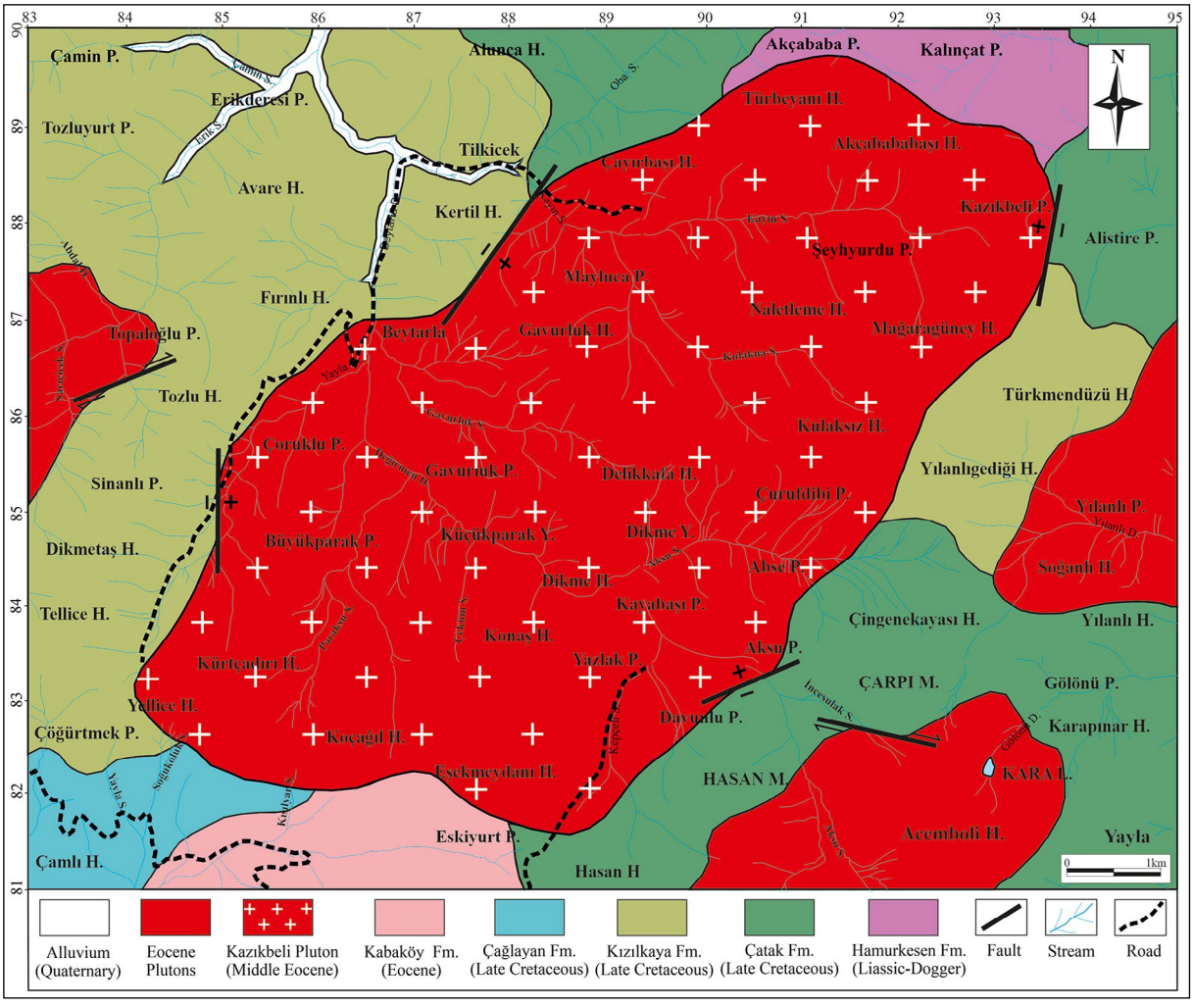

Figure 2- Geological map of the study area (modified from Güloğlu, 2022).

1993), featuring widespread exposures of dacites and pyroclastics, overlying the Çatak Formation. Another Late Cretaceous unit, the Çağlayan Formation (Güven, 1993), conformably overlies the aforementioned formations but with limited exposure in the study area's southwestern part. This formation is composed of basalt-andesite and associated pyroclastics. Unconformably above the Late Cretaceous formations lies the Eocene-aged Kabaköy Formation (Güven, 1993). This formation exhibits a distinct sequence, transitioning from nummulitic sandy limestone and tuffites through agglomerates to hornblende andesite and pyroclastics at upper levels. The Eocene-aged plutons, including Kazıkbeli Pluton intrudes all previously described formations. Quaternary alluviums represent the youngest geologic units within the study area (Figure 2).

The Kazıkbeli Pluton exhibits an elongated, elliptical shape with a northeast-southwest trending long axis (Figure 2). It covers an approximate area of 46 km², with dimensions ranging from 5-7 km in width and 8-10 km in length. The pluton displays intrusive contacts with a variety of formations spanning the Lower Jurassic to Eocene eras. These formations include the Hamurkesen Formation (Lower Jurassic), Çatak Formation (Late Cretaceous), Kızılkaya Formation (Late Cretaceous), Çağlayan Formation (Late Cretaceous), and Kabaköy Formation (Eocene). The contact zones are characterized by significant alteration, evidenced by localized epidotization and chloritization. Faulted contact zones exhibit further evidence of strike-slip and normal fault movement, with brecciated structures and crush zones prevalent in areas affected by normal faulting.

The Kazıkbeli Pluton is characterized by distinct cooling fractures, particularly around Kazıkbeli Plateau, Beytarla, Çurufdibi Plateau, Davunlu Plateau, Dikme Plateau, and Gavurluk Plateau (Figures 3a and b). These areas exhibit well-developed, sporadic crack systems and well-blocked rock structures (Figures 3a and b). In contrast, plutonic rocks near the margins display more intensive fracturing and cracking, lacking a well-blocked structure. Overall, the Kazıkbeli Pluton presents a generally robust appearance with minimal weathering. However, in weathered zones, the rocks become friable, acquiring a sandy and earthy texture (Figures 3c and d).

3. Material and Method

Within the scope of the research, a total of 50 rock samples were collected during fieldwork, and thin sections of these samples were prepared to determine detailed petrographic features under a polarizing microscope. In addition, modal analyses were conducted for 39 of these samples. In the modal analyses, counts were made for sections with grain sizes between approximately 0.5 and 0.8 mm at 1000 to 1100 points, and for sections with grain sizes between 1.0 and 1.5 mm at 1500 to 1600 points. Counting errors were calculated for the counted samples using error formulas and counts for four samples were repeated. The mineral chemistry (microprobe) analyses of two rock samples (gabbroic diorite and granodiorite) from the studied plutonic rock were performed at

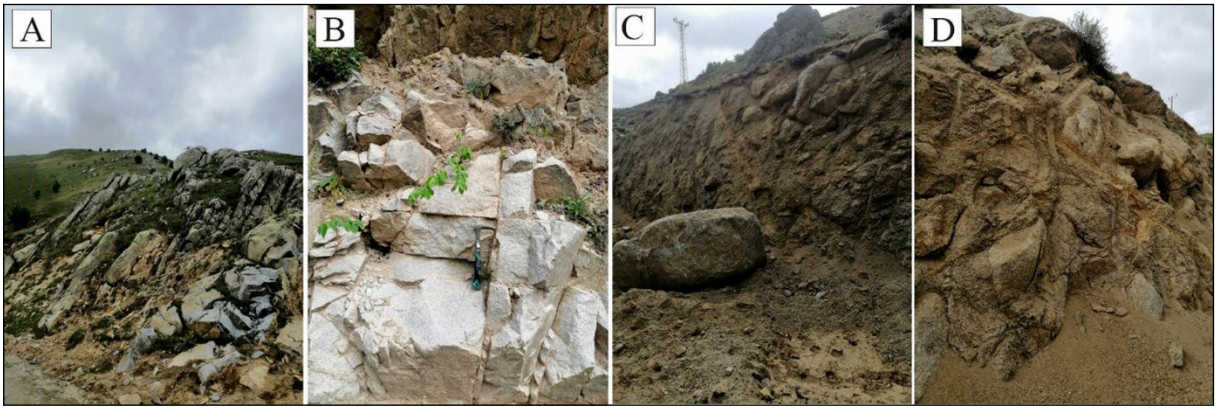

Figure 3- a-b) Cracking systems in the rocks of the Kazıkbeli Pluton, c-d) Arena formation observed in the rocks of the Kazıkbeli Pluton.

the Geological and Mineral Research Laboratory of New Mexico Tech University in the United States. The analyses of previously prepared polished section samples were conducted using a CAMECA SX 100 Electron Microprobe under conditions of 15 kV voltage and 20 nA current. The beam diameter used in the analyses was 10 µm, and counting times were set at 10 seconds for Al, Si, Ti, Ca, Mn, Fe, Mg, K, and Na elements. Electron microprobe analyses employed a 1 µm focused beam for pyroxene, amphibole, epidote, zircon and Fe-Ti oxide. To minimize Na (sodium) loss during analyses of mica, feldspar, and chlorite, a slightly defocused 10 µm beam was utilized. The standards used for measurements were diopside, kaersutite, albite, orthoclase, biotite, magnetite, and anorthite (UCB) (Nielsen and Sigurdsson, 1981).

4. Results

4.1. Petrography of the Kazıkbeli Pluton

The results of the modal analysis for the investigated plutonic rocks are presented in Table 1. The modal mineralogy is further visualized on a QAP diagram (Figure 4) and a zoning map of the pluton based on modal compositions (Figure 5).

Modal analysis data for the Kazıkbeli Pluton rock samples, plotted on the QAP diagram (Streckeisen, 1976; Figure 4), reveals a compositional spectrum encompassing diorite. Quartz diorite, tonalite, granodiorite, and monzogranite, Notably, monzogranites, the least abundant rock type, are primarily concentrated in the central regions of the pluton (Figure 5).

Granodiorites exhibit the most widespread distribution, commonly occurring around the periphery of the monzogranite zone (Figure 5). Tonalites, quartz diorites, and diorites are less prevalent compared to granodiorites and are typically situated at the pluton's margins (Figure 5). This spatial distribution suggests a compositional zonation within the Kazıkbeli Pluton.

Microscopic examination reveals that the Kazıkbeli Pluton rocks exhibit a range of textures, including

Table 1- Modal mineralogy of the Kazıkbeli Pluton, summarized by minimum, maximum, and average values obtained from modal analyses of the rock samples.

Rock type	Plagioclase	Quartz	Orthoclase	Amphibole	Biotite	Opaque minerals
Diorite						
min	63.80	1.80	3.00	11.20	0.80	2.30
max	80.40	3.70	5.20	21.40	2.20	6.10
avg	72.48	2.60	4.18	15.16	1.68	4.14
Quartz diorite						
min	56.50	6.50	3.30	13.40	0.60	4.30
max	64.00	13.95	5.82	20.50	5.70	4.80
avg	61.09	9.56	4.23	16.42	4.64	4.52
Tonalite						
min	37.10	19.72	7.40	1.90	0.90	1.35
max	62.10	30.90	21.02	14.30	8.70	3.90
avg	48.14	26.11	13.51	6.04	4.22	2.25
Granodiorite						
min	60.30	18.20	3.20	5.30	1.00	2.10
max	61.90	24.10	5.60	12.40	2.20	2.90
avg	60.90	21.27	4.43	9.63	1.53	2.67
Monzogranite						
min	26.04	26.10	21.80	1.30	1.30	0.65
max	39.10	37.00	30.00	7.70	7.39	3.00
avg	33.69	32.07	26.12	3.53	4.02	1.98
min: minimum values, max: maximum values, avg: average values						

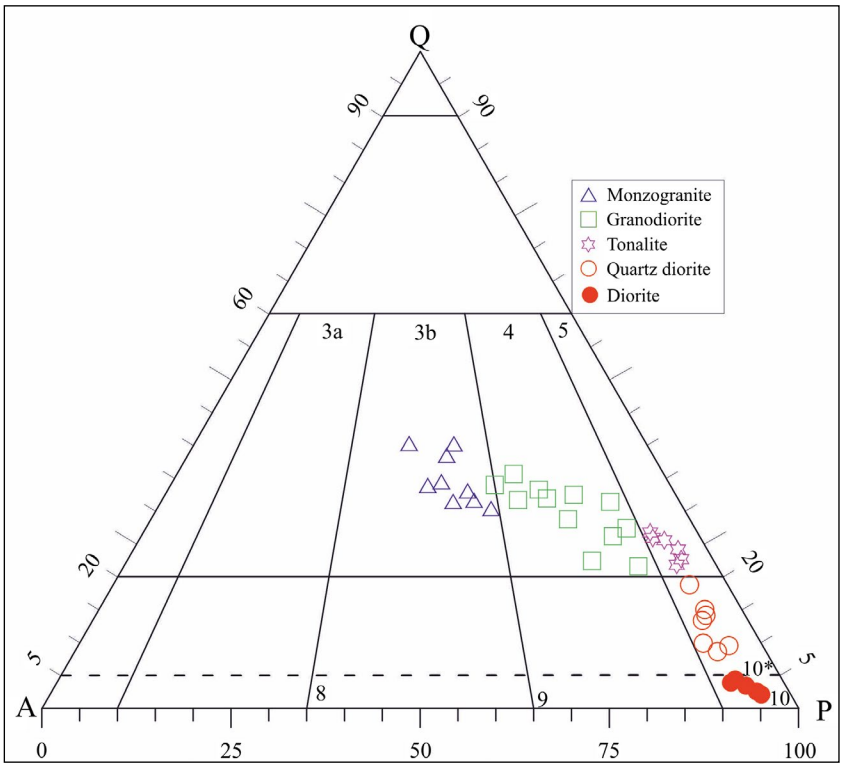

Figure 4- The QAP classification diagram (Streckeisen, 1976) illustrates the modal compositions of rock samples from the Kazıkbeli Pluton (3a: syenogranite, 3b: monzogranite, 4: granodiorite, 5: tonalite, 8: monzonite, 9: monzodiorite/gabbro, 10: diorite/gabbro, 10*: quartz diorite/gabbro).

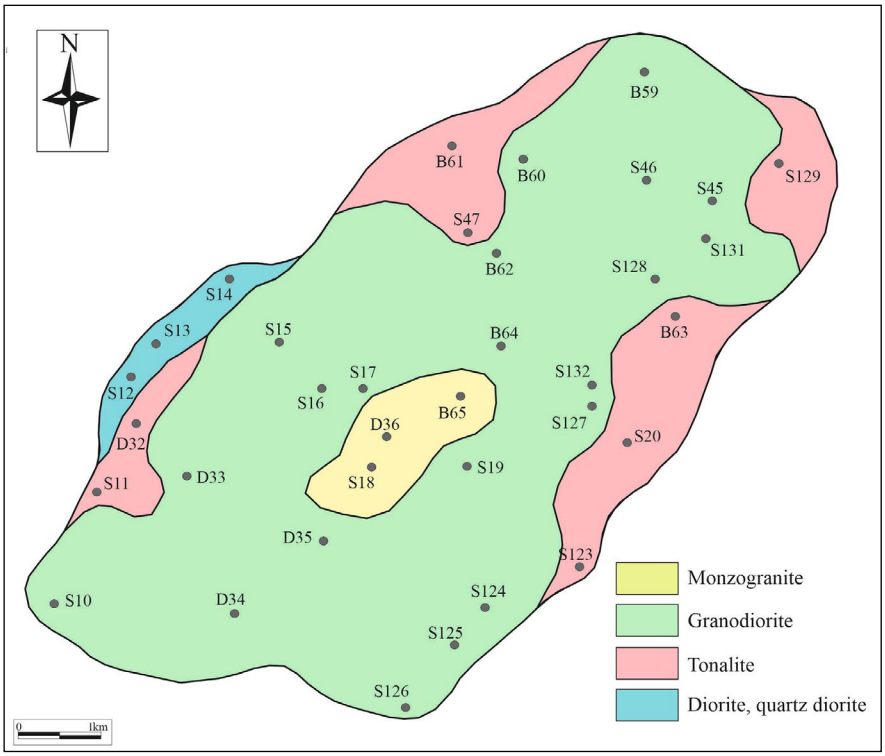

Figure 5- Locations and zoning map based on modal compositions of rock samples from the Kazıkbeli Pluton (S, B, D: sample locations).

fine- to medium-grained, porphyritic, occasionally graphic, poikilitic, and perthitic (Figures 6a-d). The primary mineral assemblage of the pluton comprises plagioclase, quartz, orthoclase, amphibole, biotite, and opaque minerals. Accessory minerals include apatite and zircon. Secondary minerals identified in the rocks are clay minerals, sericite, chlorite, and calcite.

Plagioclase is the most abundant mineral, present in all samples (26.04-80.40%; Table 1) as idiomorphic to subhedral tabular prismatic crystals (Figures 6a-d). Albite twins are commonly observed, with occasional occurrences of polysynthetic (albite-pericline) twins. Oscillatory zoning is present in some larger crystals (Figure 6d). K-feldspar (orthoclase) is anhedral to subhedral crystals and is found in rocks at a rate of 3.0-30.0% (Table 1). Karlsbad twinning is observed in some minerals, while others exhibit perthitic structures. Notably, some large orthoclase crystals enclose smaller plagioclase crystals, creating a poikilitic texture (Figure 6c). Additionally, in some instances, orthoclase fills the space between quartz and other minerals (Figure 6b). Quartz is anhedral to subhedral crystals of varying sizes. Undulatory extinction is observed in some sections, indicating a fractured and cracked structure (Figure 6c). The abundance of quartz varies between 1.8% and 37% (Table 1). Amphibole is idiomorphic to subhedral tabular prismatic crystals. Larger crystals may contain inclusions of opaque minerals and plagioclase (Figures 6a and b). Alteration in some rock samples resulted in the formation of chlorite and calcite. The abundance varies between 1.3% and 21.4% (Table 1). Biotite is idiomorphic to subhedral acicular prismatic crystals, and is found at a rate of 0.6-8.7% (Table 1). Color pleochroism is evident in some sections,

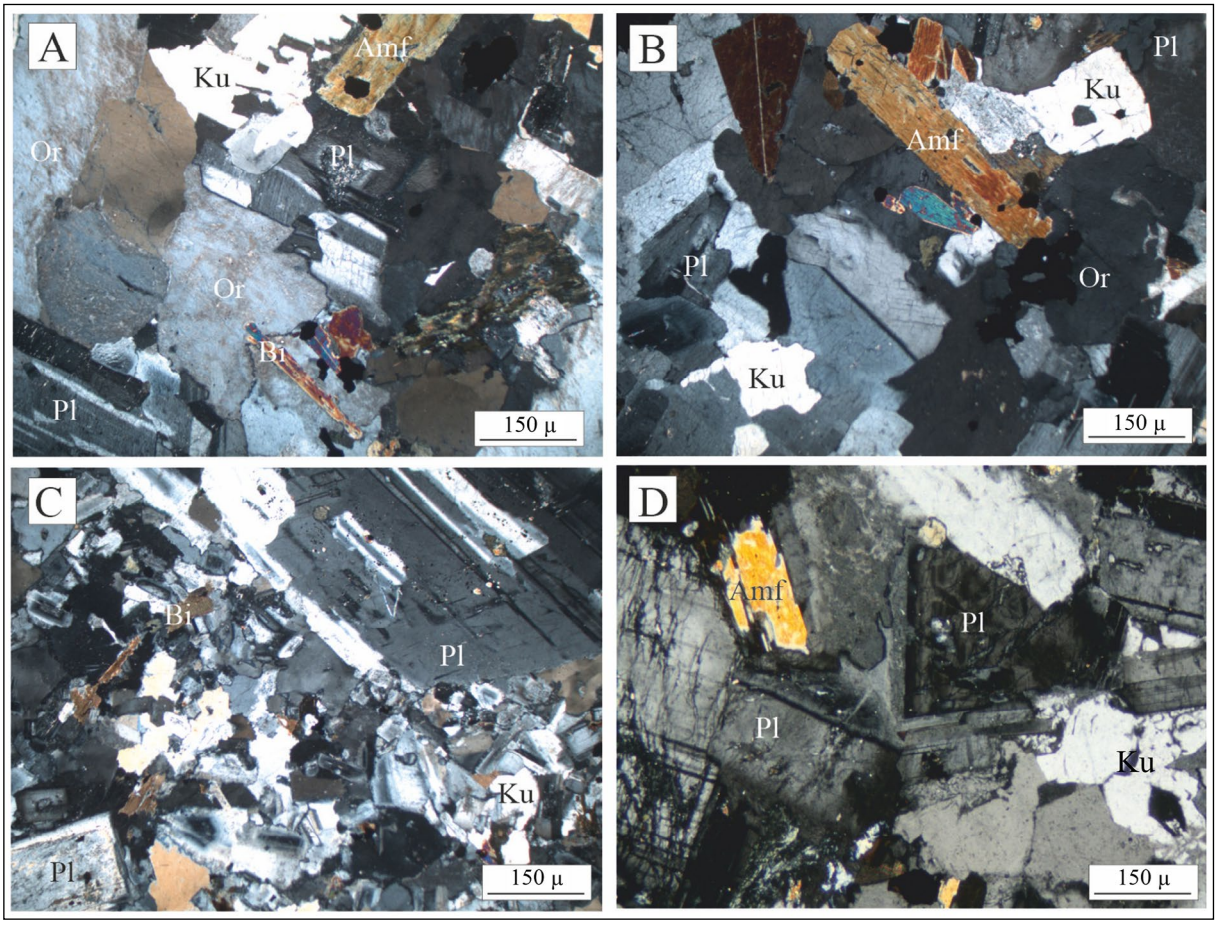

Figure 6- Microscopic features observed in the rocks of the studied pluton, a) Fine- to medium-grained texture with large orthoclase crystals, b) Granular texture, c) Poikilitic texture, characterized by small plagioclase crystals enclosed within larger plagioclase phenocrysts, d) Zoned plagioclase crystal (Cross Nicol, Pl: plagioclase, Or: orthoclase, Qz: quartz, Amp: amphibole Bt: biotite).

with partial alteration of biotite to chlorite observed in association with feldspar (Figure 6c). Apatite is typically occurs as needle-like inclusions within quartz and feldspar. Zircon is observed in almost all rocks as small, euhedral prismatic crystals. Opaque Minerals are present as euhedral and subhedral crystals, and are found at a rate of 0.7-6.1% of the studied rocks (Table 1).

4.2. Mineral Chemistry

4.2.1. Plagioclase

Microprobe analysis of plagioclase minerals in the studied Kazıkbeli Pluton reveals compositional variations between An_{26} and An_{66} (Table 2; Figure 7). Plagioclases within both mafic (gabbroic diorite) and felsic (granodiorite) lithologies exhibit SiO_2 contents ranging from 51 to 61 wt%, Al_2O_3 from 24 to 30 wt%, FeO^T from 0.2 to 0.5 wt%, and K_2O from 0.2 to 0.5 wt% (Table 2).

Plagioclases within the gabbroic diorites of the Kazıkbeli Pluton display oscillatory zoning, characterized by fluctuations in An content between An_{47} and An_{64} (Table 2).

4.2.2. K-Feldspars

Examination of Eocene-aged rocks revealed the presence of K-feldspar minerals throughout most samples. Chemical analyses of these K-feldspar minerals (Table 3) documented variations in SiO_2 (63-65 wt%), Al_2O_3 (19-20 wt%), and BaO (0.03-0.72 wt%) (Table 3; Figure 8). Notably, all K-feldspar minerals exhibited an orthoclase composition (Figure 9) with no evidence of chemical zoning within the crystals. The overall rock compositions ranged from Or_{80} to Or_{97} (Table 3; Figure 8).

4.2.3. Biotite

Microprobe analyses of biotites (Table 4) reveal TiO_2 contents ranging from 4.1 to 4.7 wt%, Al_2O_3 from 12 to 13 wt%, and MgO from 12 to 14 wt%. Mg# [$Mg/(Mg + Fe^{+2})$] and Fe# [$Fe^{+2}/(Fe^{+2} + Mg)$] ratios range from 0.52 to 0.58 and 0.42 to 0.48, respectively (Table 4). These values indicate that b iotites

Table 2- Microprobe analysis values of plagioclase**.**

Rock type	**Gabbroic diorite**								
Sample	S 13-01	S 13-02	S 13-03	S 13-04	S 13-05	S 13-06	S 13-07	S 13-08	S 13-11
(r-c)	(r)	(r)	(c)	(c)	(c)	(c)	(c)	(c)	(r)
SiO_2	55.39	54.74	51.91	54.69	51.26	54.08	53.90	53.03	50.96
Al_2O_3	27.84	27.68	30.02	27.87	30.05	28.02	28.25	28.59	30.34
FeO^T	0.35	0.33	0.44	0.48	0.37	0.36	0.38	0.51	0.35
CaO	9.92	10.45	12.71	10.17	13.02	10.81	10.90	11.26	13.33
Na_2O	5.97	5.44	4.02	5.67	3.89	5.12	4.91	4.62	3.76
K_2O	0.29	0.32	0.23	0.31	0.19	0.34	0.31	0.29	0.18
BaO	0.06	0.06	0.06	0.07	0.04	0.05	0.05	0.06	0.03
SrO	0.10	0.17	0.09	0.14	0.12	0.09	0.15	0.10	0.17
Total	99.92	99.19	99.48	99.40	98.94	98.87	98.85	98.46	99.12
Si	2.50	2.50	2.37	2.49	2.36	2.47	2.47	2.44	2.34
Al	1.48	1.49	1.62	1.50	1.63	1.51	1.52	1.55	1.64
$Fe^{(ii)}$	0.01	0.01	0.02	0.02	0.01	0.01	0.01	0.02	0.01
Ca	0.48	0.51	0.62	0.50	0.64	0.53	0.53	0.56	0.66
Na	0.52	0.48	0.36	0.50	0.35	0.45	0.44	0.41	0.34
K	0.02	0.02	0.01	0.02	0.01	0.02	0.02	0.02	0.01
An	47.08	50.54	62.74	48.90	64.18	52.78	54.08	56.40	65.51
Ab	51.28	47.61	35.91	49.33	34.70	45.24	44.09	41.87	33.44
Or	1.64	1.84	1.35	1.77	1.12	1.98	1.83	1.73	1.05
FeO^T has been measured as the total iron content. r: rim. c: center. The formulas have been calculated based on 8 oxygen.									

Table 2- Continued.

Rock type	**Granodiorite**							
Sample	S 19-01	S 19-02	S 19-03	S 19-07	S 19-08	S 19-11	S 19-12	S 19-15
(r-c)	(r)	(c)	(c)	(c)	(r)	(c)	(r)	(r)
SiO_2	56.03	55.39	55.11	59.40	60.61	57.06	61.16	59.78
Al_2O_3	26.97	27.54	27.42	24.59	24.51	26.36	23.86	25.02
FeO^T	0.47	0.48	0.49	0.30	0.24	0.33	0.26	0.32
CaO	9.28	9.63	9.52	6.29	6.04	8.39	5.40	6.83
Na_2O	6.19	5.97	5.98	8.02	8.26	6.85	8.34	7.44
K_2O	0.39	0.38	0.38	0.44	0.46	0.34	0.37	0.47
BaO	0.06	0.05	0.08	0.03	0.00	0.06	0.00	0.01
SrO	0.10	0.13	0.12	0.08	0.04	0.04	0.06	0.10
Total	99.49	99.57	99.10	99.15	100.16	99.43	99.45	99.97
Si	2.54	2.51	2.51	2.68	2.70	2.58	2.74	2.67
Al	1.44	1.47	1.47	1.31	1.29	1.40	1.26	1.32
$Fe^{(ii)}$	0.02	0.02	0.02	0.01	0.01	0.01	0.01	0.01
Ca	0.45	0.47	0.47	0.30	0.29	0.41	0.26	0.33
Na	0.54	0.53	0.53	0.70	0.71	0.60	0.72	0.64
K	0.02	0.02	0.02	0.03	0.03	0.02	0.02	0.03
An	44.30	46.11	45.78	29.49	28.05	39.59	25.80	32.75
Ab	53.48	51.73	52.04	68.05	69.41	58.50	72.10	64.56
Or	2.22	2.17	2.18	2.46	2.54	1.91	2.10	2.68
FeO^T has been measured as the total iron content. r: rim. c: center. The formulas have been calculated based on 8 oxygen.								

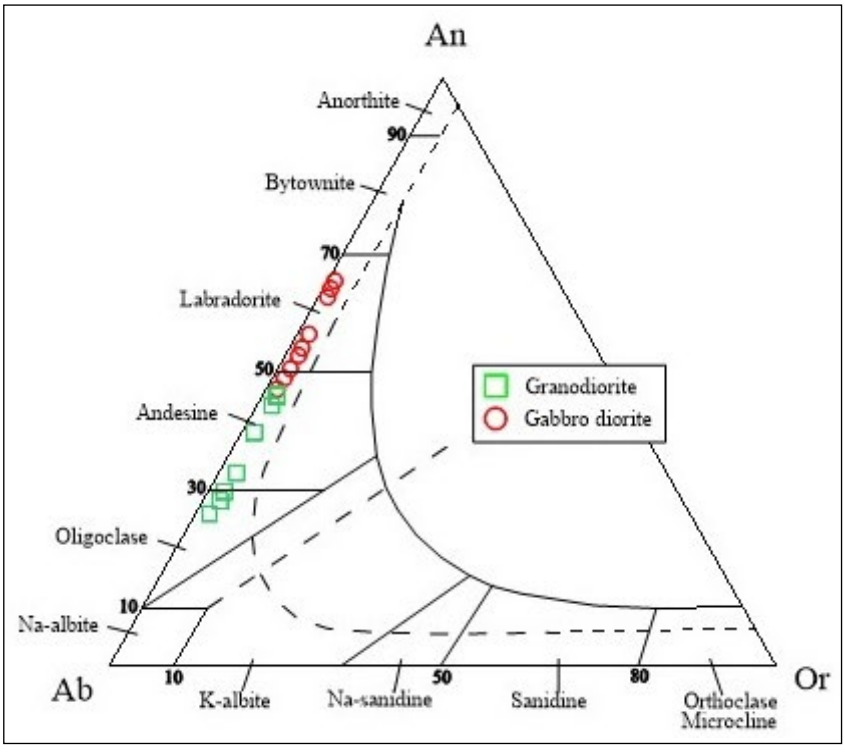

Figure 7- An-Ab-Or ternary diagram showing felspar compositions (Smith and Brown, 1988) in the studied pluton.

Table 3- Microprobe analysis values of K-feldspars.

Rock type	**Gabbroic diorite**							
Sample	S 13-1	S 13-2	S 13-3	S 13-4	S 13-5	S 13-6	S 13-7	S 13-8
(r-c)	(r)	(c)	(c)	(c)	(c)	(c)	(c)	(r)
SiO_2	64.33	64.65	64.42	64.32	64.27	64.36	64.80	64.86
Al_2O_3	18.91	19.12	19.04	19.15	19.14	19.52	19.02	19.08
FeO^T	0.30	0.12	0.10	0.10	0.26	0.16	0.09	0.15
CaO	0.11	0.13	0.08	0.11	0.09	0.27	0.10	0.08
Na_2O	1.78	1.70	2.01	1.83	2.07	2.11	1.69	1.69
K_2O	14.58	14.70	14.09	14.13	13.89	13.43	14.24	14.37
BaO	0.03	0.07	0.21	0.28	0.26	0.72	0.12	0.09
SrO	0.03	0.03	0.05	0.09	0.03	0.08	0.07	0.07
Total	100.07	100.52	100.00	100.01	100.01	100.65	100.13	100.39
Si	2.97	2.97	2.97	2.96	2.96	2.95	2.98	2.97
Al	1.03	1.03	1.03	1.04	1.04	1.05	1.03	1.03
$Fe^{(ii)}$	0.01	0.00	0.00	0.00	0.01	0.01	0.00	0.01
Ca	0.01	0.01	0.00	0.01	0.00	0.01	0.00	0.00
Na	0.16	0.15	0.18	0.16	0.18	0.19	0.15	0.15
K	0.86	0.86	0.83	0.83	0.82	0.78	0.83	0.84
Ba	0	0	0	0.01	0	0.01	0	0
An	0.53	0.63	0.39	0.54	0.44	1.34	0.50	0.40
Ab	15.57	14.86	17.75	16.36	18.39	19.02	15.21	15.10
Or	83.90	84.52	81.86	83.10	81.17	79.64	84.30	84.50
FeO^T has been measured as total iron. The formula has been calculated based on 8 oxygen. r: rim. c: center.								

Table 3- Continued.

Rock type	**Granodiorite**							
Sample	S 19-1	S 19-2	S 19-3	S 19-4	S 19-5	S 19-6	S 19-7	S 19-8
(r-c)	(r)	(c)	(c)	(c)	(c)	(c)	(c)	(r)
SiO_2	63.80	63.57	63.23	63.60	64.99	63.68	63.86	63.80
Al_2O_3	18.97	18.96	18.73	18.70	19.14	18.88	18.92	18.93
FeO^T	0.09	0.04	0.13	0.21	0.03	0.04	0.10	0.01
CaO	0.09	0.11	0.07	0.10	0.06	0.05	0.13	0.12
Na_2O	0.79	0.79	0.67	0.83	0.95	0.62	0.84	0.35
K_2O	15.86	15.69	15.62	15.57	15.70	15.74	15.21	16.28
BaO	0.18	0.51	0.45	0.24	0.21	0.40	0.54	0.29
SrO	0.05	0.07	0.03	0.05	0.08	0.06	0.10	0.03
Total	99.83	99.74	98.93	99.30	101.16	99.47	99.70	99.81
Si	2.96	2.96	2.97	2.97	2.97	2.97	2.97	2.97
Al	1.04	1.04	1.04	1.03	1.03	1.04	1.04	1.04
$Fe^{(ii)}$	0.00	0.00	0.01	0.01	0.00	0.00	0.00	0.00
Ca	0.00	0.01	0.00	0.01	0.00	0.00	0.01	0.01
Na	0.07	0.07	0.06	0.08	0.08	0.06	0.08	0.03
K	0.94	0.93	0.93	0.93	0.92	0.94	0.90	0.97
Ba	0	0.01	0.01	0	0	0.01	0.01	0.01
An	0.44	0.54	0.35	0.50	0.29	0.25	0.66	0.60
Ab	7.01	7.07	6.10	7.46	8.40	5.63	7.69	3.15
Or	92.55	92.39	93.55	92.05	91.31	94.11	91.65	96.26
FeO^T has been measured as total iron. The formula has been calculated based on 8 oxygen. r: rim. c: center.								

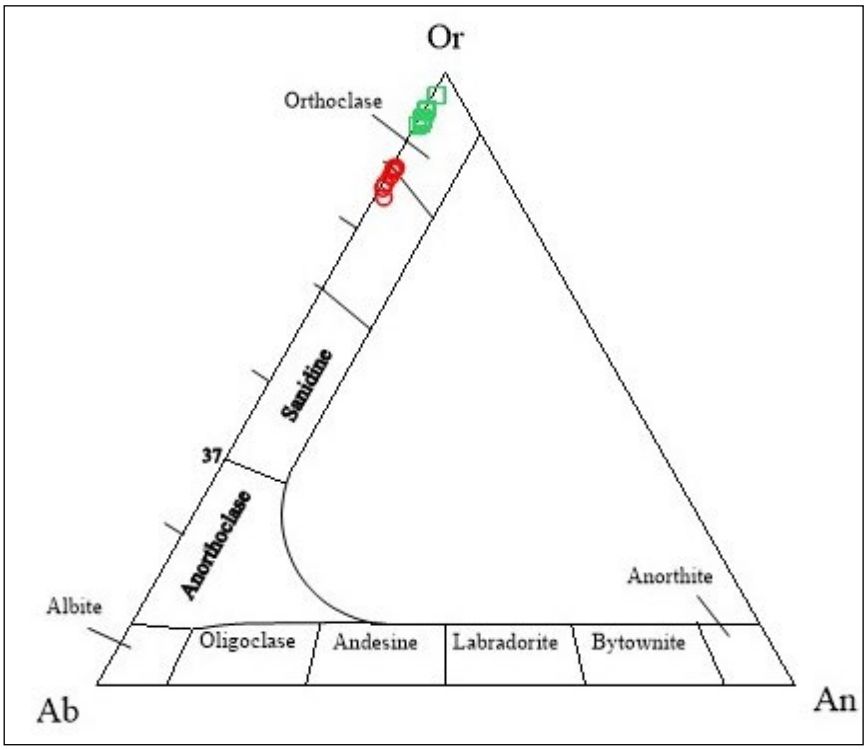

Figure 8- Classification diagram for K-feldspars using the An-Ab-Or diagram (from Deer et al., 1992).

Table 4- The microprobe analysis results of biotites.

Rock type	**Gabbroic diorite**			**Granodiorite**						
Sample	S 13-1	S 13-2	S 13-3	S 19-1	S 19-2	S 19-3	S 19-4	S 19-5	S 19-6	S 19-7
(r-c)	(r)	(c)	(c)	(r)	(c)	(r)	(c)	(c)	(c)	(c)
SiO_2	37.85	37.38	37.91	36.69	36.02	37.49	36.94	36.79	37.11	37.14
TiO_2	4.59	4.64	4.69	4.12	4.14	4.30	4.11	4.43	4.68	4.61
Al_2O_3	12.40	12.47	12.71	13.04	12.67	12.20	12.60	12.52	12.60	12.75
FeO^T	18.02	18.23	17.57	19.44	19.31	18.96	19.28	18.70	18.51	19.03
MnO	0.26	0.26	0.22	0.22	0.17	0.19	0.18	0.33	0.31	0.32
MgO	13.31	12.95	13.84	11.81	11.57	12.03	12.21	12.08	12.80	12.34
CaO	0.04	0.05	0.04	0.20	0.27	0.19	0.11	0.27	0.06	0.09
Na_2O	0.12	0.13	0.14	0.15	0.16	0.15	0.16	0.14	0.14	0.15
K_2O	9.50	9.44	9.50	8.67	9.11	8.73	9.10	9.02	9.32	9.28
Cl	0.19	0.26	0.24	0.32	0.33	0.30	0.25	0.27	0.41	0.27
F	0.40	0.38	0.44	0.14	0.14	0.18	0.19	0.32	0.31	0.35
Total	96.68	96.19	97.30	94.80	93.89	94.72	95.13	94.87	96.25	96.33
Si	5.65	5.62	5.60	5.62	5.60	5.73	5.65	5.62	5.59	5.59
Ti	0.52	0.52	0.52	0.47	0.48	0.49	0.47	0.51	0.53	0.52
Al	2.18	2.21	2.21	2.36	2.32	2.20	2.27	2.26	2.23	2.26
$Fe^{(ii)}$	2.25	2.29	2.17	2.49	2.51	2.42	2.46	2.39	2.33	2.40
Mn	0.03	0.03	0.03	0.03	0.02	0.02	0.02	0.04	0.04	0.04
Mg	2.96	2.90	3.05	2.70	2.68	2.74	2.78	2.75	2.87	2.77
Ca	0.01	0.01	0.01	0.03	0.04	0.03	0.02	0.04	0.01	0.01
Na	0.03	0.04	0.04	0.04	0.05	0.04	0.05	0.04	0.04	0.04
K	1.81	1.81	1.79	1.69	1.81	1.70	1.77	1.76	1.79	1.78
Cl	0.05	0.07	0.06	0.08	0.09	0.08	0.06	0.07	0.10	0.07
F	0.19	0.18	0.21	0.07	0.07	0.09	0.09	0.15	0.15	0.17
Fe#	0.43	0.44	0.42	0.48	0.48	0.47	0.47	0.46	0.45	0.46
Mg#	0.57	0.56	0.58	0.52	0.52	0.53	0.53	0.54	0.55	0.54
FeO^T has been measured as total Fe. The formulas have been calculated based on 22 oxygen. r: rim. c: center.										

crystallized as solidified melt products with compositions between annite and phlogopite endmembers, plotting close to the magnesium-rich end of the phlogopite solid solution series (Figure 9a). Furthermore, microprobe analyses classify biotites within the C field of the $FeO^{(T)}$-Al_2O_3 diagram (Figure 9b), coexisting with pyroxenes and hornblendes based on the $FeO^{(T)}$ - Al_2O_3-MgO triangular diagram (Figure 9c). Finally, the MgO-FeO+MnO-TiO_2*10 triangular diagram classifies these biotites as primary brown biotites (A field) (Figure 9d).

4.2.4. Amphibole

Microprobe analyses of amphiboles from the studied plutonic rocks (Table 5) reveal Al_2O_3 contents ranging from 4.6 to 6.2 wt%, SiO_2 contents from 47.1 to 50.2 wt%, and Mg# values between 0.63 and 0.73. Classification diagrams indicate that all amphiboles belong to the calcic amphibole field based on the Na versus (Ca+Na) ratio (Figure 10a) and exhibit a magnesiohornblende composition according to Leake et al. (1997) (Figure 10b).

4.3. Crystallization Conditions of Magma Forming the Kazıkbeli Pluton

The formation and stability of minerals within magma are primarily governed by variations in temperature (T), pressure (P), and oxygen fugacity (fO_2). Determining these intensive variables (T, P, fO_2) offers crucial insights into the crystallization history of magma. Thermodynamic principles enable the prediction of mineral phases that crystallize

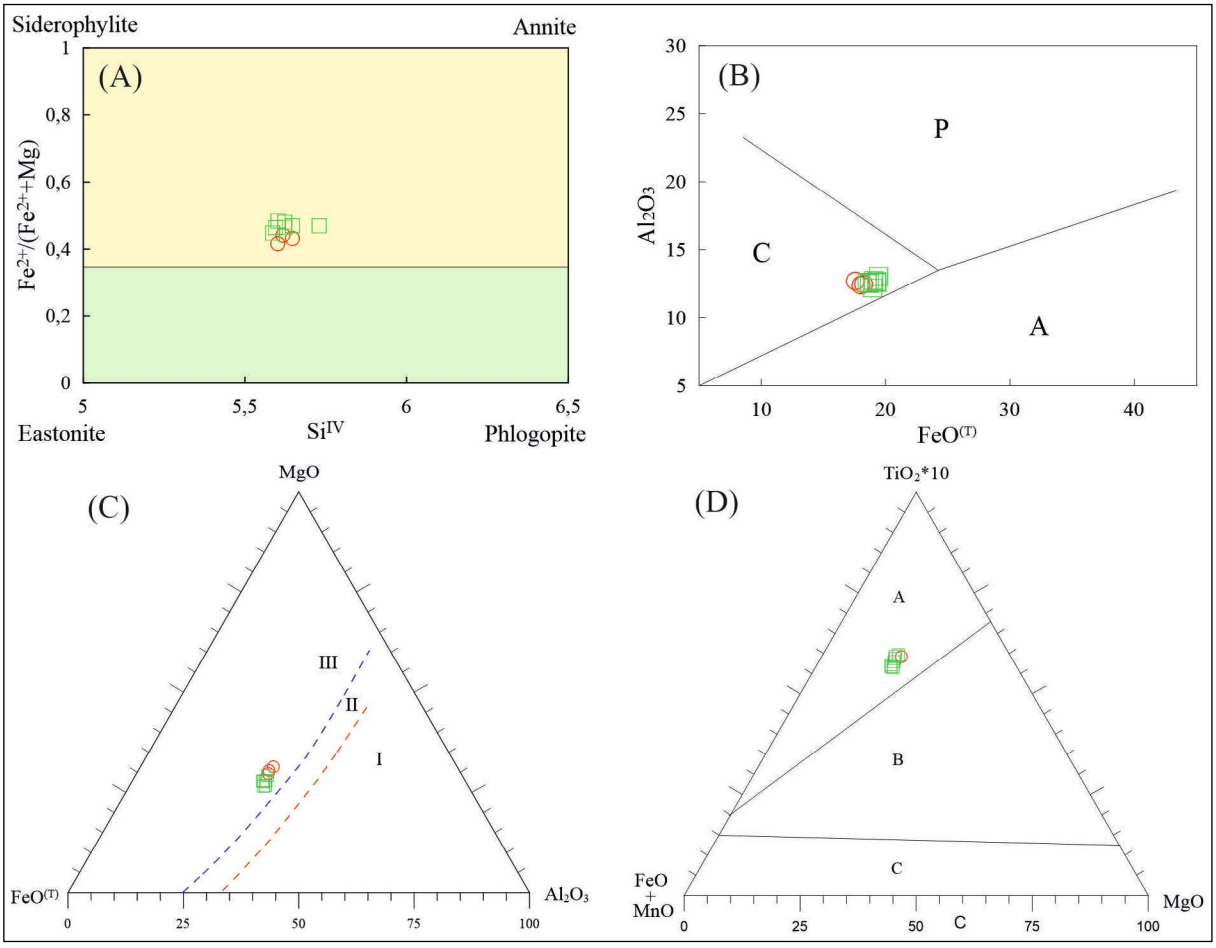

Figure 9- The composition of biotites in the studied rocks: a) Si^{IV} - (Fe^{+2}/Fe^{+2} + Mg) diagram (Parsons et al., 1991), b) $FeO^{(T)}$-Al_2O_3 diagram (Abdel-Rahman, 1994) (C: biotites associated with subduction, P: biotites after continental collision, A: biotites formed in anorogenic regions), c) $FeO^{(T)}$-Al_2O_3-MgO triangle diagram (I: biotites associated with muscovite and topaz, II: biotites associated with other mafic minerals, III: biotites associated with hornblende, pyroxene, or olivine), d) MgO-FeO+MnO-TiO_2*10 triangle diagram (Speer, 1984) (A: primary brown biotites, B: primary re-equilibrated green and greenish-brown biotites, C: secondary green biotites).

Table 5- Microprobe analysis results of amphiboles.

Rock type	Gabbroic diorite				Granodiorite					
Sample	S 13-1	S 13-2	S 13-3	S 13-4	S 19-1	S 19-2	S 19-3	S 19-4	S 19-5	S 19-6
(r-c)	(r)	(c)	(c)	(c)	(r)	(c)	(c)	(c)	(c)	(c)
SiO_2	49.83	50.24	49.61	50.21	47.64	47.14	48.87	48.14	48.65	49.12
TiO_2	0.77	0.89	1.07	0.83	1.30	1.15	0.80	0.88	1.13	0.83
Al_2O_3	4.57	4.68	4.76	4.72	5.82	6.20	5.09	5.57	5.01	4.95
FeO^T	15.39	14.80	14.48	14.93	16.43	16.35	16.02	16.14	14.24	15.63
MnO	0.53	0.54	0.47	0.51	0.54	0.55	0.49	0.47	0.43	0.57
MgO	14.27	14.55	14.50	14.62	13.02	13.18	13.26	12.97	14.29	13.86
CaO	11.09	11.15	11.17	10.99	11.15	10.90	11.27	11.34	11.40	10.97
Na_2O	1.22	1.12	1.13	1.14	1.50	1.50	0.97	1.05	1.30	1.27
K_2O	0.42	0.38	0.51	0.37	0.64	0.66	0.48	0.59	0.52	0.47
Total	98.09	98.35	97.70	98.32	98.04	97.63	97.25	97.15	96.97	97.67
Si	7.25	7.27	7.23	7.27	7.01	6.96	7.22	7.13	7.15	7.20
Ti	0.08	0.10	0.12	0.09	0.14	0.13	0.09	0.10	0.12	0.09
Al	0.78	0.80	0.82	0.80	1.01	1.08	0.89	0.97	0.87	0.85
$Fe^{(ii)}$	1.87	1.79	1.76	1.81	2.02	2.02	1.98	2.00	1.75	1.92
Mn	0.07	0.07	0.06	0.06	0.07	0.07	0.06	0.06	0.05	0.07
Mg	3.10	3.14	3.15	3.15	2.85	2.90	2.92	2.86	3.13	3.03
Ca	1.73	1.73	1.74	1.70	1.76	1.72	1.78	1.80	1.79	1.72
Na	0.69	0.63	0.64	0.64	0.86	0.86	0.56	0.60	0.74	0.72
K	0.08	0.07	0.09	0.07	0.12	0.12	0.09	0.11	0.10	0.09
Fe#	0.70	0.69	0.73	0.64	0.82	0.73	0.74	0.78	0.84	0.71
Mg#	0.70	0.72	0.71	0.73	0.63	0.67	0.67	0.65	0.68	0.69

FeO^T has been measured as total Fe. The formulas have been calculated based on 23 oxygen. r: rim. c: center.

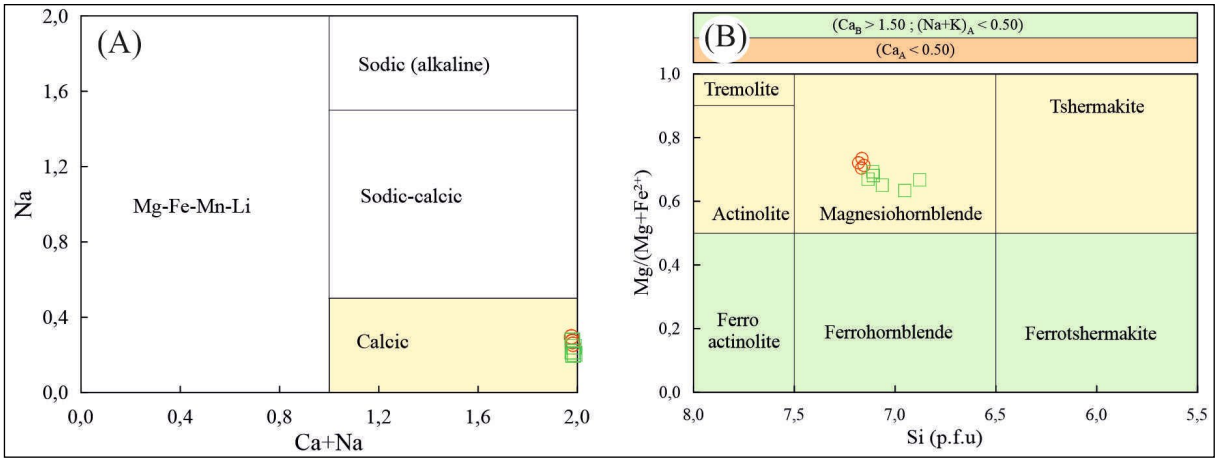

Figure 10- a-b) Composition of amphiboles in the studied plutonic rocks (Leake et al., 1997).

under specific conditions. Conversely, the mineral assemblage and composition within a rock can be utilized to infer the P-T conditions during its formation (thermobarometry). The accuracy of thermodynamic calculations hinges on the identification and propagation of errors throughout all stages of P-T estimation. Typically, thermobarometric calculations exhibit uncertainties of ±30-50°C for temperature and

±1-0.5 kbar for pressure. Notably, the limited diversity of mineral assemblages encountered in plutonic rocks presents a significant challenge for precise P-T determinations.

The ubiquity of amphibole-plagioclase pairs in calcalkaline plutonic rocks makes them a popular choice for thermobarometric calculations (Hammarstrom and Zen, 1986; Hollister et al., 1987; Johnson and Rutherford, 1989; Blundy and Holland, 1990; Schmidt, 1992; Holland and Blundy, 1994). Fortunately, the mineral assemblage of the studied plutons is amenable to this approach due to the presence of both amphibole and plagioclase. However, caution is warranted. Post-magmatic processes such as actinolite transformation, chloritization, and the formation of opaque minerals can compromise the integrity of hornblende compositions (Hammarstrom and Zen, 1986). Consequently, components exhibiting alteration must be meticulously excluded from thermobarometric calculations.

This investigation employed a suite of thermobarometric calculations to elucidate the pressure (P), temperature (T), oxidation state (fO_2) conditions and water contents prevailing during the crystallization of the studied plutonic rocks. Mineral assemblages, including amphibole, plagioclase, biotite, K-feldspar, quartz, and Fe-Ti oxides, served as the basis for these calculations.

4.3.1. Geobarometer

In order to determine the crystallization pressures of the rocks from the Kazıkbeli Pluton, a multi-equilibrium approach was employed. This approach utilized established barometers, including the amphibole-$Al^{(T)}$ (Hammarstrom and Zen, 1986; Hollister et al., 1987; Johnson and Rutherford, 1989; Schmidt, 1992), amphibole (Ridolfi et al., 2010; Ridolfi and Renzulli, 2012), and biotite (Uchida et al., 2007) barometers were employed to determine crystallization pressures. The results of these barometers are presented in Table 6 and detailed below.

Pressure estimation in plutonic rocks is often achieved through the analysis of $Al^{(T)}$ in amphiboles. This approach relies on the established positive correlation between $Al^{(T)}$ content and pressure, as documented by Hammarstrom and Zen (1986), Hollister et al. (1987), Johnson and Rutherford

Table 6- The pressure estimates calculated using amphibole-plagioclase, amphibole and biotite for the Kazıkbeli pluton.

	P (kbar) (Hammarstrom and Zen, 1986)	**P (kbar) (Hollister et al., 1987)**	**P (kbar) (Schmidt, 1992)**	**P (kbar) (Ridolfi et al., 2010)**	**P (kbar) (Ridolfi and Renzulli, 2012)**	**P (kbar) (Uchida et al., 2007)**
Minerals	Amphibole-Plagioclase			Amphibole		Biotite
Gabbroic diorite						
Min	0.07	0.04	0.68	0.50	0.60	0.08
Max	0.15	0.08	0.84	0.60	0.70	0.18
Avg	0.12	0.06	0.76	0.55	0.65	0.14
SD (±)	0.04	0.03	0.07	0.06	0.06	0.05
Min Depth (km)	0.3	0.1	2.5	1.9	2.2	0.3
Max Depth (km)	0.6	0.3	3.1	2.2	2.6	0.7
Granodiorite						
Min	0.33	0.11	1.01	0.60	0.70	0.13
Max	1.44	1.25	2.06	0.90	1.00	0.61
Avg	0.78	0.62	1.44	0.75	0.82	0.36
SD (±)	0.44	0.48	0.42	0.10	0.12	0.18
Min Depth (km)	1.2	0.4	3.7	2.2	2.6	0.5
Max Depth (km)	5.3	4.6	7.6	3.3	3.7	2.3

Min: Minimum, Max: Maximum, Avg: Average, SP (±): Standard deviation.
Depth was taken as 1kbar = 3.7 km for the continental crust (Tulloch and Challis. 2000).

(1989), and Schmidt (1992). Various calibrations have been developed to convert $Al^{(T)}$ values into pressure estimates, each with specific applicability depending on the crystallization environment. For instance, the Johnson and Rutherford (1989) calibration (P (kbar) = 4.28 $Al^{(T)}$ - 3.54) is best suited for volcanic or high-pressure plutonic settings. Conversely, the calibrations proposed by Hollister et al. (1987) (P (kbar) = 5.64 $Al^{(T)}$ - 4.76) and Hammarstrom and Zen (1986) (P (kbar) = 5.03 $Al^{(T)}$ - 3.92) are more accurate for high-pressure plutonic environments. Finally, the calibration by Schmidt (1992) (P (kbar) = 4.76 $Al^{(T)}$ - 3.01) is preferred for low-pressure settings. These variations in calibration effectiveness highlight the influence of the surrounding mineral assemblage (plagioclase, K-feldspar, biotite, pyroxene, magnetite, ilmenite, and potentially sphene) on the equilibrium relationships that govern $Al^{(T)}$ incorporation in amphiboles.

The estimation of crystallization pressures employed the aluminum-in-hornblende barometer technique applied to amphiboles, as detailed in Table 6. This approach yielded a range of pressures dependent on the specific calibration chosen. Hammarstrom and Zen (1986) proposed a pressure range expressed as 5.03 $Al^{(T)}$ - 3.92 kbar. Their calculations resulted in values between 0.07 and 0.15 kbar for gabbroic diorites and between 0.33 and 1.44 kbar for granodiorites (Table 6). Hollister et al. (1987) established a distinct pressure range of 5.64 $Al^{(T)}$ - 4.76 kbar, 0.04-0.08 kbar for gabbroic diorites and 0.11-1.25 kbar for granodiorites (Table 6). Finally, Schmidt (1992) presented a pressure estimation of 4.76 $Al^{(T)}$ - 3.01 kbar, translating to a range of 0.68 to 0.84 kbar for gabbroic diorites and 1.01 to 2.06 kbar for granodiorites (Table 6).

The pressure conditions under which the plutonic rocks crystallized were estimated using amphibole mineral chemistry data. Barometric formulas developed by Ridolfi et al. (2010) and Ridolfi and Renzulli (2012) (Table 6) were employed for these calculations. Ridolfi et al. (2010) based calculations resulted in a pressure range of 0.5–0.9 kbar, with distinct values of 0.5-0.6 kbar for gabbroic diorites and 0.6–0.9 kbar for granodiorites (Table 6). Similarly, the Ridolfi and Renzulli (2012) method yielded a pressure range of 0.6 to 1.0 kbar, with 0.6 to 0.7 kbar for gabbroic diorites and 0.7 to 1.0 kbar for granodiorites (Table 6).

Biotite crystallization pressures were determined using the empirical equation established by Uchida et al. (2007). This formula, calibrated based on $Al^{(T)}$ content obtained from mineral chemistry analyses, yielded a pressure range of 0.08-0.61 kbar for the studied plutonic rocks (Table 6). Notably, pressures varied from 0.08 to 0.18 kbar for gabbroic diorites and from 0.13 to 0.61 kbar for granodiorites (Table 6).

4.3.2. Geothermometer

Amphibole-plagioclase (Holland and Blundy, 1994), amphibole (Ridolfi et al., 2010; Ridolfi and Renzulli, 2012), and biotite (Luhr et al., 1984) thermometers were utilized to estimate crystallization temperatures. The results obtained from these thermometers are presented in Table 7 and detailed below.

Magma crystallization temperatures were estimated using the Blundy and Holland (1990) amphibole-plagioclase thermometer. This approach relies on two equilibrium reactions involving edenite, tremolite, pargasite, albite, and quartz. The calculation employs a formula (T = 0.667P - 48.98 + Y / (-0.0429 - 0.008314 LnK)) that incorporates pressure (P) derived from the assumption of equilibrium crystallization between amphibole and plagioclase. Within the formula, Y and K values are determined based on the composition of the amphibole (Xab, Si content). However, this specific thermometer is only applicable under certain conditions: (i) Equilibrium crystallization of amphibole-plagioclase must occur alongside quartz, K-feldspar, biotite, pyroxene, Fe-Ti oxide, and sphene. (ii) Plagioclase feldspar composition must be less calcic than An_{92} (albite molar fraction exceeding 0.08). (iii) Coexisting amphibole must have a cationic Si content below 7.8 atoms per formula unit. This type of amphibole-plagioclase thermometer is typically suited for estimating temperatures within the range of 500 °C to 1100 °C.

The calculated temperatures in the pluton, using the proposed formulas, range between 742-824°C for the studied rocks. Specifically, temperatures range

from 742 °C to 744 °C for gabbroic diorites and from 757 °C to 824 °C for granodiorites (Table 7).

Equilibrium crystallization temperatures within the studied plutonic rocks were estimated using amphibole compositions and the thermometers developed by Ridolfi et al. (2010) and Ridolfi and Renzulli (2012) (Table 7). The Ridolfi et al. (2010) formulation yielded a temperature range of 738-797 °C for the entire pluton, with distinct values of 740-751 °C for gabbroic diorites and 738-797 °C for granodiorites (Table 7).

Amphibole compositions were employed to estimate equilibrium crystallization temperatures using the equations proposed by Ridolfi and Renzulli (2012). The calculated temperatures range from 712 °C to 804 °C throughout the pluton, with specific values of 744 °C to 748 °C for gabbroic diorites and 712 °C to 804 °C for granodiorites (Table 7).

Biotite mineral chemistry analyses were employed to calculate crystallization temperatures within the studied plutonic rocks using the formulas proposed by Luhr et al. (1984) (Table 7). These calculations yielded a temperature range of 721-783 °C, with specific values of 768-783 °C for gabbroic diorites and 721-766 °C for granodiorites (Table 7).

4.3.3. Oxygen Fugacity

Crystallization processes within magmatic systems are significantly influenced by oxygen fugacity (fO_2), which represents the partial pressure of oxygen. This parameter exerts control over the pressure-temperature relationships governing melt behavior and dictates the stability fields of rock-forming minerals (Wones, 1989; Ridolfi et al., 2010). Notably, fO_2 exhibits a positive correlation with temperature, typically increasing as temperatures rise. Additionally, the oxygen content within silicate melts is influenced by the source of the heat driving the process and the rate of gas mixing (Wones, 1989). However, due to the slow cooling rates experienced by granitic magmas, direct determination of their original fO_2 values remains elusive. Consequently, researchers rely on relative approaches and calculations to estimate this crucial parameter (Wones, 1989; Anderson and Smith, 1995; Kemp, 2004).

Oxygen fugacity (ΔNNO) within the studied plutonic rocks was estimated using amphibole compositions and the oxybarometry models developed by Ridolfi et al. (2010) and Ridolfi and Renzulli (2012) (Table 8). The Ridolfi et al. (2010) formulation yielded ΔNNO values ranging from 1.3 to 2.0, with distinct values of 1.8-2.0 for gabbroic diorites and 1.3-1.7 for granodiorites (Table 8). In contrast, the Ridolfi and Renzulli (2012) model resulted in a ΔNNO range of 0.2 to 1.0, with values of 0.4-0.6 for gabbroic diorites and 0.2-1.0 for granodiorites (Table 8).

Oxygen fugacity (fO_2) in the studied rocks was determined using the Wones (1989) method, which relies on pressure and temperature values. These

Table 7- The temperature estimates calculated using amphibole-plagioclase, amphibole and biotite for the Kazıkbeli pluton.

	T (°C) (Blundy and Holland, 1990)	**T (°C) (Ridolfi et al., 2010)**	**T (°C) (Ridolfi and Renzulli, 2012)**	**T (°C) (Luhr et al., 1984)**
Minerals	Amphibole-Plagioclase	Amphibole	Amphibole	Biotite
Gabbroic diorite				
Min	742	740	744	768
Max	744	751	748	783
Avg	743	746	746	773
SD (±)	1	5	2	9
Granodiorite				
Min	757	738	712	721
Max	824	797	804	766
Avg	784	766	756	736
SD (±)	29	22	35	18

pressure and temperature values were calculated using the approach outlined by Ridolfi et al. (2010). The calculations yielded a range of fO_2 values from -13.8 to -12.5, with distinct values of -13.1 to -13.4 for gabbroic diorites and -12.5 to -13.8 for granodiorites (Table 8).

Oxygen fugacity (fO_2) values in the studied rocks were calculated using the temperature data derived from the method established by Wones (1989) (Table 8). These calculations yielded a range of fO_2 values from -16.14 to -14.31, with distinct values observed in gabbroic diorites (-14.72 to -14.31) and granodiorites (-16.14 to -14.78) (Table 8).

4.3.4. Water Content

The water content of magmas containing amphiboles remains a topic of debate, with reported values ranging from 2-3 wt% (Luhr et al., 1984) to a mean of 5 wt% (Eggler, 1972; Helz, 1973; Naney, 1983) or even 6 wt% (Merzbacher and Eggler, 1984). In this study, calculations based on the amphiboles within the studied samples yielded water content estimates between 4.4 and 7.8 wt%. The presence of hydrous mafic minerals (amphibole, biotite), titanite, and apatite in the studied plutons serves as an indicator of a magma rich in water and other volatile components. Notably, high-temperature magmas with such compositions may ascend to relatively shallow depths within the continental crust before complete crystallization (Helmy et al., 2004).

The water contents of amphiboles in the studied rocks were determined using the hydrometer formulas developed by Ridolfi et al. (2010) and Ridolfi and Renzulli (2012) (Table 8). Hydration states of amphiboles within the studied rocks were assessed using the hydrometer calculations proposed by Ridolfi et al. (2010) and Ridolfi and Renzulli (2012). The results are presented in Table 8.

Average water contents of amphiboles in the studied rocks, determined using Ridolfi et al. (2010) method, range from 3.7% to 4.5% (Table 8). Specifically, they vary between 3.9% and 4.3% for gabbroic diorites and 3.7% and 4.5% for granodiorites (Table 8).

Amphibole water contents within the studied rocks were determined using the method established by Ridolfi and Renzulli (2012) (Table 8). These calculations revealed an average water content range of 4.4% to 5.7%, 4.5% to 4.6% for gabbroic diorites. Granodiorites exhibited a wider range, varying between 4.4% and 5.7% (Table 8).

4.4. Disequilibrium Parameters

The interplay between mineral compositions and textural features observed in rocks offers valuable insights into the various types of disequilibrium encountered during magma evolution. Factors such as cooling, decompression, and magma mixing can trigger variations in temperature, pressure, and composition, ultimately driving the magmatic system

Table 8- The oxygen fugacity and water content estimates calculated using amphibole and biotite for the Kazıkbeli pluton.

	DNNO (Ridolfi et al., 2010)	**DNNO (Ridolfi and Renzulli, 2012)**	**fO_2 (Ridolfi et al., 2010)**	**fO_2 (Wones, (1989)**	**H_2O (Ridolfi et al., 2010)**	**H_2O (Ridolfi and Renzulli, 2012)**
Minerals	Amphibole			Biotite	Amphibole	
Gabbroic diorite						
Min	1.80	0.40	-13.40	-14.72	3.90	4.50
Max	2.00	0.60	-13.10	-14.31	4.30	4.60
Avg	1.90	0.48	-13.20	-14.58	4.13	4.55
SD (±)	0.08	0.10	0.14	0.24	0.17	0.06
Granodiorite						
Min	1.30	0.20	-13.80	-16.14	3.70	4.40
Max	1.70	1.00	-12.50	-14.78	4.50	5.70
Avg	1.52	0.52	-13.13	-15.67	4.17	4.83
SD (±)	0.16	0.46	0.47	0.54	0.31	0.51

towards disequilibrium (Nixon, 1988; Rutherford and Hill, 1993; Simonetti et al., 1996; Perugini et al., 2003). Petrographic or textural criteria serve as key indicators of textural disequilibrium. These include the presence of sieved plagioclase crystals (Dungan and Rhodes, 1978), the coexistence of normal and sieved plagioclase within a single sample (Stimac and Pearce, 1992; Venezky and Rutherford, 1997), and the occurrence of rounded and embayed crystals (Stimac and Pearce, 1992). Compositional criteria provide another window into disequilibrium processes. The presence of both normally and reversely zoned crystals within the same sample serves as a diagnostic feature (Sakuyama, 1981). These variations in zoning patterns reflect the changing chemical composition of the magma as it undergoes disequilibrium.

Textural, petrographic, and mineral compositional features within the studied rocks provide compelling evidence for disequilibrium processes and compositional zoning, particularly in plagioclase (Figure 6). Oscillatory zoning observed in plagioclase crystals is a well-established indicator of disequilibrium (Figure 6d). Additionally, the occasional presence of sieve textures within these minerals offers further support for this interpretation. The occurrence of reverse zoning in some plagioclase grains, particularly noteworthy, and the coexistence of both normally and reversely zoned plagioclase crystals within the same sample (Figure 11) constitute definitive evidence for disequilibrium crystallization. Furthermore, the presence of K-feldspar poikiloblasts enclosing plagioclase, amphibole, and opaque minerals (Figure 6) represents another textural feature suggestive of disequilibrium crystallization.

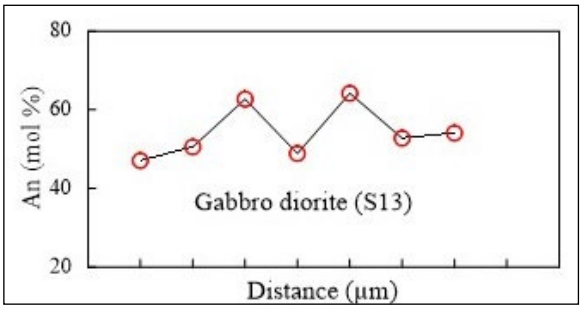

Figure 11- The observed variations in An (%) of zoned plagioclase minerals in the studied pluton (Symbols are as in Figure 4).

Normal zoning patterns in plagioclase crystals are readily attributable to fractional crystallization processes. However, the origin of reverse zoning remains a topic of debate, with several competing explanations: (i) Blundy and Cashman (2001) propose that reverse zoning can arise due to an increase in both temperature and pressure within a water-saturated magma system. (ii) Alternatively, Blundy et al. (2006) suggest that reverse zoning may develop during the ascent of water-saturated magmas as a consequence of rising temperatures. (iii) Couch et al. (2001) and Streck (2008) posit that back-mixing of cooler magmas with hotter, inflowing magmas can induce temperature increases, leading to reverse zoning in plagioclase. The studied samples exhibit a wide compositional range (An_{26-66}) within the rims of individual plagioclase crystals (Table 2). This significant compositional variability within a single sample is consistent with a complex origin for the plagioclase, likely influenced by magma mixing processes (Wallace and Carmicheal, 1994).

4.5. Evolution of Magma within the Crust

The Eastern Pontide (EP) has predominantly experienced a compressional tectonic regime throughout its geological history, particularly intensifying since the Paleozoic-Mesozoic transition. This compression resulted in the development of fracture systems oriented in the NE-SW and NW-SE directions. Notably, the elongated axes of plutons within the EP exhibit a strong correlation with these primary fracture trends. Gedikoğlu (1979) first documented this observation, and subsequent studies in the region have further corroborated this relationship (Kaygusuz et al., 2008, 2012, 2016, 2020, 2021).

Field observations reveal that the Kazıkbeli Pluton exhibits an elongated, elliptical shape and is situated subparallel to regional NE-SW trending faults. This geometry suggests emplacement within a regional zone of tectonic weakness. The pluton exhibits sharp, incompatible contacts with the surrounding fine-grained country rocks. Notably, these country rocks occasionally display porphyritic and granophyric textures, and in some locations, xenoliths derived from the country rocks have been incorporated into the pluton. These combined observations, including

the shape, contact relationships, and presence of xenoliths, are indicative of emplacement at relatively shallow crustal depths.

The presence of Early Eocene aged (~ 55 Ma) adakitic rocks in the Eastern Pontides corresponds to the last stage of the arc-continent collision and is associated with a collisional or post-collisional origin (Topuz et al., 2005, 2011; Karslı et al., 2010, 2011). In the Middle Eocene (~ 46-40 Ma), the presence of I-type, metaluminous, medium to high-K and occasionally shoshonitic plutonic rocks are linked to collisional eventsand subsequent geodynamic processes. Pre-existing studies (Boztuğ et al., 2004; Topuz et al., 2005; Arslan and Aslan, 2006; Karslı et al., 2007; Kaygusuz et al., 2011; Arslan et al., 2013; Aydınçakır, 2014; Kaygusuz and Öztürk, 2015; Yücel et al., 2017; Temizel et al., 2018) indicated that the geochemical signatures are consistent with derivation from enriched lithospheric mantle or lower continental crust, or a mixture of both. The Eocene magmatism is attributed to a tensional regime associated with collision, post-collisional crustal thickening, and lithospheric delamination (Kaygusuz et al., 2011; Karslı et al., 2012; Temizel et al., 2012; Arslan et al., 2013; Aslan et al., 2014; Yücel et al., 2017). Lithospheric delamination following slab break-off is proposed as a mechanism for the formation of the Kazıkbeli plutonic rocks. The developing delamination enabled the upward movement (local or regional) of the asthenosphere and provided a hot asthenosphere thermal anomaly, leading to the partial melting of the chemically enriched lithospheric mantle and the formation of magmas that led to the formation of Middle Eocene rocks. After that, thinning and fracture systems formed in the crust due to tectonic extension allowed these melts to move upwards within the crust. During magma ascent, a chamber formed at a depth of approximately 3-5 km where fractional crystallization and magma mixing events occurred. Barometer estimates based on mineral assemblages and petrographic features (Table 6) suggest these magma chambers existed at depths ranging from 1 to 8 km (Figure 12). Magma mixing is further supported

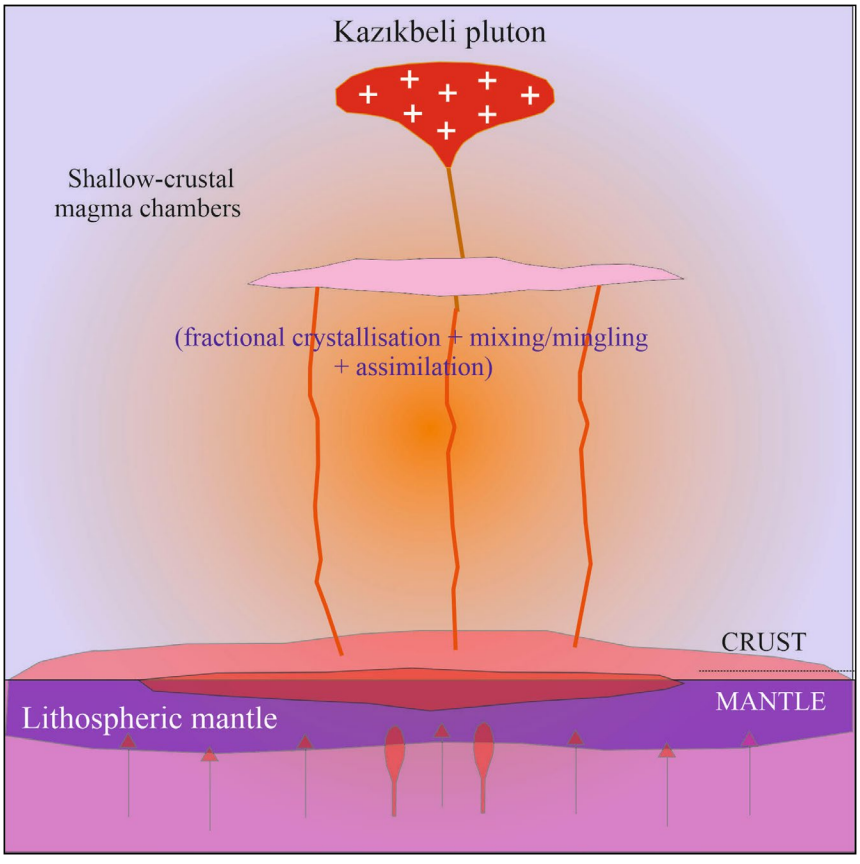

Figure 12- Schematic cross-section of the studied Kazıkbeli pluton within the crust, showing its emplacement and development.

by textural features such as sieve texture and zoning. Finally, estimates of oxygen fugacity indicate oxidizing conditions prevailed during crystallization at this depth.

5. Discussion

The amphibole-plagioclase and amphibole barometers employed in this study yielded comparable pressure values ranging from 0.04 to 2.06 kbar (Table 3). While the pressures estimated from the biotite barometer were slightly lower (0.08-0.61 kbar), they remained within the same general range. These findings are consistent with observations reported in the literature, where pressure values obtained using the hornblende-Al barometer for plutons align well with geological features and emplacement depths (Tulloch and Challis, 2000). In light of the convergent pressure estimates obtained from various methods and the qualitative observations from the studied plutons, the emplacement pressure can be confidently constrained to a range of approximately 1-2 kbar. Notably, the calcic nature of the amphiboles in the pluton, characterized by $Al^{(T)}$ values below 2.0, further supports a shallow intrusion environment (Hammarstrom and Zen, 1986). Textural features observed within the plutons, such as the presence of porphyritic textures and mineral regrowth (Figure 6), also lend credence to a shallow emplacement depth.

Solidus temperatures, typically exceeding 700°C, are often estimated using thermometers like the amphibole-plagioclase method (Anderson, 1996). The amphibole-plagioclase thermometer (Holland and Blundy, 1994) in this study gave temperature estimates within a narrow range (742-824 °C) and similar to the amphibole thermometer (738-804 °C) (Table 7). Additionally, the biotite thermometer (Luhr et al., 1984) yielded lower temperature estimates (721-783 °C) (Table 7). However, these low biotite-derived temperatures likely reflect re-equilibration with subsolidus intracrystalline variations during feldspar cooling (Toksoy-Köksal, 2016). The broad temperature range obtained from the hornblende-plagioclase thermometer may also suggest re-equilibration processes in slowly cooling plutonic rocks.

Mineral chemistry plays a critical role in establishing the emplacement depth of plutonic rocks. Microprobe analyses of amphiboles from the Kazıkbeli Pluton (Table 5) reveal compositions that plot within the low-pressure field of Figure 13. This geochemical signature is indicative of crystallization at relatively shallow depths within the Earth's crust.

Pressure estimates derived from amphibole-plagioclase, amphibole, and biotite barometry in the studied plutonic rocks range from 0.04 to 2.06 kbar (Table 6). These values are comparable to pressures reported for other Eocene plutons in the Eastern Pontide: 1-3.8 kbar for the Sarıçiçek and Dölek plutons (Karslı et al., 2007) and 0.1-2.8 kbar for the Kemerlikdağı, Aydıntepe, and Pelitli Plutons (Kaygusuz et al., 2020). However, pressures in the studied plutons are generally lower compared to a broader range documented for the Sarıçiçek, Dölek, Üzengili, Arslandede, and Sorkunlu plutons (0.3-8.2 kbar; Eyüboğlu et al., 2017). Supporting the interpretation of shallow emplacement depths are the compositional characteristics of the amphiboles. These amphiboles are classified as calcic, with $Al^{(T)}$ values typically less than 2.0. According to Hammarstrom and Zen (1986), such low $Al^{(T)}$ contents are indicative of crystallization at shallow crustal levels. Furthermore, textural features observed in the studied rocks, such as the presence of graphic intergrowths, further corroborate the shallow emplacement depths.

Thermometry calculations utilizing amphibole, amphibole-plagioclase, and biotite compositions in

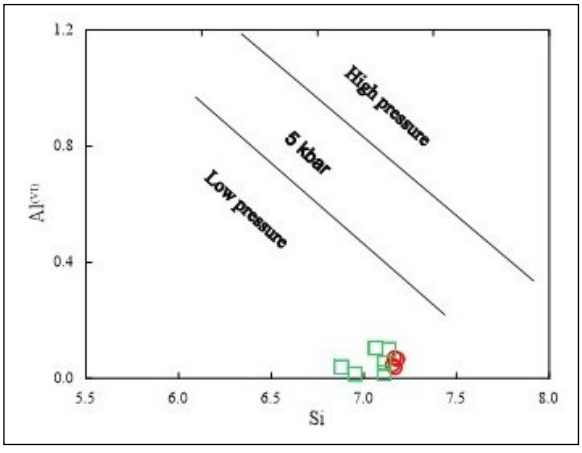

Figure 13- Composition and pressure range of amphiboles in the studied Kazıkbeli Pluton.

the investigated plutonic rocks yielded temperature values ranging from 712 to 824 °C (Table 7). This temperature range is consistent with values reported for other plutons of similar age within the Eastern Pontide: 617-768 °C for the Sarıçiçek and Dölek plutons (Karslı et al., 2007) and 616-1172 °C for the Kemerlikdağı, Aydıntepe, and Pelitli Plutons (Kaygusuz et al., 2020). However, the temperature range for the studied plutons falls within a narrower window compared to the broader range documented for the Sarıçiçek, Dölek, Üzengili, Arslandede, and Sorkunlu plutons (388-1196 °C; Eyüboğlu et al., 2017).

It is well established that thermometers like the amphibole-plagioclase method typically yield temperatures exceeding the solidus temperature (typically >700°C) (Anderson and Smith, 1995). In the case of the studied plutonic rocks, the temperatures derived from the amphibole-plagioclase thermometer fall below the expected solidus value. This observation suggests that the amphiboles may have undergone sub-solidus re-equilibration processes, as described by Moazzen and Droop (2004).

Biotite compositions within the studied plutonic rocks exhibit characteristics suggestive of a potential mantle origin. These biotites display intermediate Al^{IV} content (2.18-2.36 formula units per biotite; f.u.b.) and partially high Mg# values (0.52-0.58) (Figure 14). These compositional features partially resemble biotites documented in plutons with established mantle sources, which typically exhibit Al^{IV} contents of 2.3-2.4 f.u.b. and Mg# exceeding 0.60.

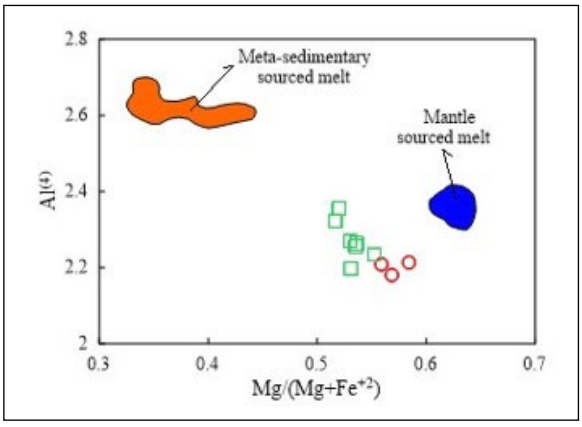

Figure 14- The Al^4 versus $Mg/(Mg+Fe^{+2})$ diagram for biotites in the studied rocks used to distinguish between two end-member melt fields: meta-sedimentary (Kemp, 2001) and mantle-derived (Kemp, 2004).

Direct determination of the original oxygen fugacity (fO_2) in granitic magmas is challenging due to the effects of post-crystallization processes during gradual cooling (Wones, 1989; Anderson and Smith, 1995; Kemp, 2004). As a consequence, researchers rely on relative approaches and calculations to estimate fO_2 values. In the studied plutonic rocks, the calculated $\log_{10} fO_2$ values range from -12.5 to -16.14. Notably, these values exhibit good agreement with those reported for the Eocene Sarıçiçek and Dölek plutons (-15 to -21; Karslı et al., 2007).

The presence of hydrous mafic minerals (amphibole) alongside apatite and titanite in the studied rocks suggests a magma enriched in water and other volatile components. Such high-temperature, water-rich magmas are capable of ascending to shallow crustal depths while remaining partially molten (Helmy et al., 2004). The water content of amphibole-bearing magmas remains a topic of debate. While Luhr et al. (1984) reported values around 2-3%, other studies suggest an average closer to 5% (Eggler, 1972; Helz, 1973; Naney, 1983), with Merzbacher and Eggler (1984) proposing an average of 6%. Notably, the water content estimates derived from the analyzed amphiboles in the studied plutons fall within a range of 3.7 to 5.7 wt%.

Thermobarometric calculations utilizing mineral compositions revealed a wide range of pressure (0.04-2.06 kbar) and temperature (712-824 °C) estimates within the studied plutonic rocks (Tables 6 and 7). These combined observations suggest the emplacement of a water-rich magma derived from the continental crust at relatively shallow depths within the crust, likely in the range of ~1 to 8 km.

6. Results

The Kazıkbeli Pluton is an elongated, elliptical intrusion oriented in a NE-SW direction, encompassing an area of approximately 46 km². It exhibits lithological variability, ranging from gabbroic diorite to granite. The rocks of the pluton are composed of plagioclase (An_{26-66}), orthoclase (Or_{80-97}), quartz, amphibole, biotite, and Fe-Ti oxides.

The Kazıkbeli rocks display a textural spectrum, encompassing fine- to medium-grained, porphyritic, poikilitic, and occasionally microlitic and graphic textures. Amphibole compositions vary in Mg# (0.63-0.73), and biotites exhibit Mg# values ranging from 0.52 to 0.58. Calculated crystallization temperatures derived from amphibole and biotite data range from 712°C to 824°C. Pressure estimates suggest emplacement at relatively shallow crustal depths (~1 to 8 km), with values ranging from 0.04 to 2.06 kbar. Oxygen fugacity (fO_2) values exhibit minimal variation, falling within a range of -12.5 to -13.8. Water contents estimated from amphiboles range between 3.7% and 5.7%.

In light of the combined geochemical and textural data, the Kazıkbeli Pluton is interpreted to have solidified at relatively shallow crustal depths, likely within a range of ~1 to 8 km.

Acknowledgement

This research was financially supported by the Scientific Research Projects Unit of Gümüşhane University through project codes 20.F5114.01.04 and 22.F5114.02.03. The authors would like to express their sincere gratitude to Hüseyin Enes Atay, Muhammet Emin Ay, and Mertcan Yılmaz for their invaluable assistance during fieldwork. The authors are also grateful to editor Halim Mutlu, reviewer Zafer Aslan and two anonymous reviewers for their constructive criticism and comments, which significantly improved the quality of this manuscript.

References

Abbott Jr., R. N. 1985. Muscovite-bearing granites in the AFM liquidus projection. Canadian Mineralogist, 23, 553-561.

Abdel–Rahman, A. M. 1994. Nature of biotites from alkaline, calc-alkaline, and peraluminous magmas. Journal of Petrology 35, 525-541.

Ağar, Ü. 1977. Demirözü (Bayburt) ve Köse (Kelkit) bölgesinin jeolojisi. Doktora tezi, İstanbul Üniversitesi, İstanbul (unpublished).

Anderson, J. L. 1996. Status of thermobarometry in granitic batholiths. Trans Royal Society Edinburgh, Earth Sciences, 87, 125-138.

Anderson, J. L., Smith, D. R. 1995. The effects of temperature and fO_2 on the Al-in hornblende barometer. American Mineralogist 80, 549-559.

Arslan, M., Aslan, Z. 2006. Mineralogy, petrography and whole-rock geochemistry of the Tertiary granitic intrusions in the eastern Pontides, Turkey. Journal of Asian Earth Sciences 27, 177-193.

Arslan, M., Temizel, İ., Abdioğlu, E., Kolaylı, H., Yücel, C., Boztuğ, D., Şen, C. 2013. ^{40}Ar–^{39}Ar dating, whole-rock and Sr–Nd–Pb isotope geochemistry of post-collisional Eocene volcanic rocks in the southern part of the Eastern Pontides (NE Turkey): Implications for magma evolution in extension-induced origin. Contributions to Mineralogy and Petrology 166, 113–142.

Arslan, M., Temizel, İ., Ackerman, L., Yücel, C., Abdioğlu Yazar, E. 2022. Highly siderophile element and Os isotope systematics of the Cenozoic volcanic rocks from the Eastern Pontides, NE Turkey: Constraints on the origin and evolution of subcontinental mantle-derived magmas. Lithos 410–411.

Aslan, Z., Arslan, M., Temizel, İ., Kaygusuz, A. 2014. K-Ar dating, whole-rock and Sr-Nd isotope geochemistry of calc-alkaline volcanic rocks around the Gümüşhane area: Implications for post-collisional volcanism in the Eastern Pontides, Northeast Turkey. Mineralogy and Petrology 108, 245–267.

Aydınçakır, E. 2014. The Petrogenesis of Early-Eocene non-adakitic volcanism in NE Turkey: Constraints on geodynamic implications**.** Litho**s** 208, 361-377.

Aydınçakır, E., Gündüz, R., Yücel, C. 2020. Emplacement conditions of magma(s) forming Jurassic plutonic rocks in Gümüşhane (Eastern Pontides, Turkey). Bullettin of the Mineral Research and Exploration 162, 175–196.

Aydınçakır, E., Yücel, C., Ruffet, G., Gücer, M. A., Akaryalı, E., Kaygusuz, A. 2022. Petrogenesis of post-collisional Middle Eocene volcanism in the Eastern Pontides (NE, Turkey): Insights from geochemistry, whole-rock Sr-Nd-Pb isotopes, zircon U-Pb and ^{40}Ar-^{39}Ar geochronology. Geochemistry 125871. https://doi.org/10.1016/j.chemer.2022.125871.

Aydınçakır, E., Yücel, C., Kaygusuz, A., Bilici, Ö., Yi, K., Jeong, Y-Z., Güloğlu, Z. S. 2023. Magmatic evolution of the Calc-alkaline Middle Jurassic igneous rocks in the Eastern Pontides, NE Turkey: Insights from geochemistry, whole-rock Sr-Nd-Pb, in situ zircon Lu-Hf isotopes, and U-Pb geochronology. International Geology Review 65, 20, 3146–3167.

Blundy, J. D., Holland, T. J. B. 1990. Calcic amphibole equilibria and a new amphibole-plagioclase geothermometer, Contributions to Mineralogy and Petrology, 104, 208-224.

Blundy, J., Cashman, K. 2001. Ascent driven crystallization of dacite magmas at Mount St. Helens, 1980-1986. Contributions to Mineralogy and Petrology 140, 631-650.

Blundy, J., Cashman, K., Humhreys, M. 2006. Magma heating by decompression-driven crystallization beneath andesite volcanoes. Nature 443, 76-80.

Boztuğ, D., Jonckheere, R., Wagner, G.A., Yeğingil, Z. 2004. Slow Senonian and fast Palaeocene–Early Eocene uplift of the granitoids in the Central eastern Pontides, Turkey: Apatite fission–track results. Tectonophysics 382, 213–228.

Boztuğ, D., Erçin, A. İ., Kuruçelik, M. K., Göç, D., Kömür, I., İskenderoğlu, A. 2006. Geochemical characteristics of the composite Kaçkar batholith generated in a Neo-Tethyan convergence system, Eastern Pontides, Turkey. Journal of Asian Earth Sciences 27, 286–302. https://doi.org/10.1016/j.jseaes.2005.03.008.

Couch, S., Sparks, R. S. J., Carroll, M. R. 2001. Mineral disequilibrium in lavas explained by convective self-mixing in open magma chambers. Nature 411, 1037-1039.

Çoğulu, E. 1975. Gümüşhane ve Rize granitik plutonlarının mukayeseli petrojeolojik ve jeokronolojik etüdü. Unpublished Doctoral Thesis, İstanbul Tech. Univ.

Deer, W. A., Howie, R. A., Zussman, J. 1992. An introduction to the rock forming minerals, (second edition), London, Longman, p, 696.

Dokuz, A. 2011. A slab detachment and delamination model for the generation of Carboniferous high-potassium I-type magmatism in the Eastern Pontides, NE Turkey: The Köse composite pluton. Gondwana Research 19, 926–944.

Dokuz, A., Sünnetçi, K. 2019. Jurassic acidic magmatism. in a back-arc setting, eastern Sakarya Zone, Turkey: Geochemical constraints and an evolutionary model: Lithos 10.1016/j.lithos.2019.02.022.

Dungan, M. A., Rhodes, J. M. 1978. Residual glasses and melt inclusions in basalts from DSDP Legs 45 and 46: Evidence for magma mixing. Contributions to Mineralogy and Petrology 67, 417-431.

Eggler, D. H. 1972. Water-saturated and undersaturated melting relations in a paricutin andesite and an estimate of water content in the natural magma, Contributions to Mineralogy and Petrology 34, 261-271.

Eyüboğlu, Y., Dudas, F. O., Santosh, M., Xiao, Y., Yi, K., Chatterjee, N., Wu, F. Y., Bektaş, O. 2016. Where are the remnants of a Jurassic Ocean in the Eastern Mediterranean Region? Gondwana Research v. 33, p. 63–92.

Eyüboğlu, Y., Dudas, F. O., Thorkelson, D., Zhu, D. C., Liu, Z., Chatterjee, N., Yi, K., Santosh, M. 2017. Eocene granitoids of northern Turkey: Polybaric magmatism in an evolving arc–slab window system. Gondwana Research.

Eyüboğlu, Y., Dudas, F. O., Santosh, M., Eroğlu-Gümrük, T., Akbulut, K., Yi, K., Chatterjee, N. 2018. The final pulse of the Early Cenozoic adakitic activity in the Eastern Pontides Orogenic Belt (NE Turkey): An integrated study on the nature of transition from adakitic to non-adakitic magmatism in a slab window setting. Journal of Asian Earth Sciences 157, 141–165.

Eyüboğlu, Y., Dudas, F. O., Zhu, D.C., Liu, Z., Chatterjee, N. 2019. Late Cretaceous I- and A-type magmas in eastern Turkey: Magmatic response to double-sided subduction of Paleo- and Neo-Tethyan lithospheres. Lithos 326–327, 39–70.

Gedikoğlu, A. 1979. Harşit (Giresun-Doğankent) granit karmaşığının jeokronolojik etüdü. Türkiye Jeoloji Bilimsel ve Teknik Kurultayı Bildiri Özleri Kitabı, 33, 59-60.

Gücer, M. A., Sarı, E. 2021. Karbonifer Pamuktaş Plütonu'nun petrografisi, jeokimyası ve petrolojik özellikleri, Bayburt (KD Türkiye). Yerbilimleri, 41(2), 85-120.

Güloğlu, Z. S. 2022. Eosen yaşlı Kazıkbeli Plütonu'nun (Kürtün-Gümüşhane) petrografisi, petrokimyası, U-Pb zirkon jeokronolojisi, tüm-kayaç Sr-Nd-Pb ve zirkon Lu-Hf izotop jeokimyası ve petrolojisi. Doktora tezi, Gümüşhane Üniversitesi, Lisansüstü Eğitim Enstitüsü, Gümüşhane (unpublished).

Güven, İ. H. 1993. Doğu Pontidler'in 1/ 250 000 ölçekli kompilasyonu, Maden Tetkik ve Arama Genel Müdürlüğü, Ankara.

Hammarstrom, J. M., Zen, E. 1986. Aluminum in hornblende: An empirical igneous geobarometer, American Mineralogist 71, 1297-1313.

Helmy, H. M., Ahmed, A. F., El Mahallawi, M. M., Ali, S. M. 2004. Pressure, temperature and oxygen fugacity conditions of calc-alkaline granitoids, Eastern Desert of Egypt, and tectonic implications. Journal of African Earth Sciences 38, 255-268.

Helz, R. T. 1973. Phase relations of basalts in their melting ranges at PH_2O=5 kb as a function of oxygen fugacity, Journal of Petrology 14, 249-302.

Holland, T. J. B., Blundy, J. D. 1994. Non-ideal interactions in calcic amphiboles and their bearing on amphibole-plagioclase thermometry. Contribution to Mineralogy and Petrology 116, 433-447.

Hollister, L. S., Grisson, G. C., Peters, E.K., Stowell, H. H., Sisson, V. B. 1987. Confirmation of the empirical calibration of aluminum in amphibole with

pressure of solidification of calc-alkaline plutons. American Mineralogist 72, 231-239.

Ilbeyli, N. 2008. Geochemical characteristics of the Sebinkarahisar granitoids in the Eastern Pontides, northeast Turkey: Petrogenesis and tectonic implications. International Geology Review 50, 563–582.

Johnson, M. C., Rutherford, M. J. 1989. Experimental calibration of the aluminum in-hornblende geobarometer with application to Long Valley Caldera (California) volcanic rocks, Geology 17, 837-841.

Karslı, O., Chen, B., Aydın, F., Şen, C. 2007. Geochemical and Sr-Nd-Pb isotopic compositions of the Eocene Dölek and Sariçiçek Plutons, Eastern Turkey: Implications for magma interaction in the genesis of high-K calc-alkaline granitoids in a post-collision extensional setting. Lithos 98, 67–96.

Karslı, O., Dokuz, A., Uysal, I., Aydın, F., Chen, B., Kandemir, R., Wijbrans, J. 2010. Relative contributions of crust and mantle to generation of Campanian high-K calc-alkaline I-type granitoids in a subduction setting, with special reference to the Harşit Pluton, Eastern Turkey. Contributions to Mineralogy and Petrology 160, 467–487.

Karslı, O., Ketenci, M., Uysal, İ., Dokuz, A., Aydın, F., Chen, B., Kandemir, R., Wijbrans, J. 2011. Adakite-like granitoid porphyries in the Eastern Pontides, NE Turkey: Potential parental melts and geodynamic implications. Lithos 127, 354–372.

Karslı, O., Uysal, İ., Ketenci, M., Dokuz, A., Kandemir, R., Wijbrans, J. 2011. Adakite-like granitoid porphyries in the Eastern Turkey: potential parental melts and geodynamic implications. Lithos 127, 354-372.

Karslı, O., Dokuz, A., Uysal, İ., Ketenci, M., Chen, B., Kandemir, R. 2012. Deciphering the shoshonitic monzonites with I-type characteristic, the Sisdağı pluton, NE Turkey: magmatic response to continental lithospheric thinning. Journal of Asian Earth Sciences 51, 45-62.

Karslı, O., Dokuz, A., Kandemir, R. 2017. Zircon Lu-Hf isotope systematics and U–Pb geochronology, whole-rock Sr-Nd isotopes and geochemistry of the early Jurassic Gokcedere pluton, Sakarya Zone-NE Turkey: a magmatic response to roll-back of the Paleo-Tethyan oceanic lithosphere. Contributions to Mineralogy and Petrology 172, 31.

Kaygusuz, A. 2000. Torul ve çevresinde yüzeylenen kayaçların petrografik ve jeokimyasal incelenmesi, Doktora tezi, Karadeniz Teknik Üniversitesi Fen Bilimleri Enstitüsü, Trabzon (unpublished).

Kaygusuz, A., Öztürk, M. 2015. Geochronology, geochemistry, and petrogenesis of the Eocene Bayburt intrusions, Eastern Pontides, NE Turkey: Evidence for lithospheric mantle and lower crustal sources in the high-Kcalc-alkalinemagmatism. Journal Asian Earth Sciences 108, 97–116.

Kaygusuz, A., Şahin, K. 2016. Petrographical, geochemical and petrological characteristics of Eocene volcanic rocks in the Mescitli area, Eastern Pontides (NE Turkey), Journal of Engineering Research and Applied Science, 5 (2), 473-486.

Kaygusuz, A., Siebel, W., Şen, C., Satır, M. 2008. Petrochemistry and petrology of I-type granitoids in an arc setting: The composite Torul pluton, Eastern Pontides, NE Turkey. International Journal Earth Sciences 97, 739–764 .

Kaygusuz, A., Arslan, M., Siebel, W., Şen, C. 2011. Geochemical and Sr-Nd isotopic characteristics of post-collisional calc-alkaline volcanics in the eastern pontides (NE Turkey). Turkish Journal of Earth Sciences 20, 137–159.

Kaygusuz, A., Arslan, M., Siebel, W., Sipahi, F., Ilbeyli, N. 2012. Geochronological evidence and tectonic significance of Carboniferous magmatism in the southwest Trabzon area, eastern Pontides, Turkey. International Geology Review 54, 1776–1800.

Kaygusuz, A., Arslan, M., Sipahi, F., Temizel, İ. 2016. U–Pb zircon chronology and petrogenesis of Carboniferous plutons in the northern part of the Eastern Pontides, NE Turkey: Constraints for Paleozoic magmatism and geodynamic evolution. Gondwana Research 39, 327–346.

Kaygusuz, A., Merdan Tutar, Z., Yücel, C. 2017. Mineral chemistry, crystallization conditions and petrography of Cenozoic volcanic rocks in the Bahçecik (Torul/Gümüşhane) area, Eastern Pontides (NE Turkey). Journal of Engineering Research and Applied Science, 6 (2), 641-651.

Kaygusuz, A., Yücel, C., Arslan, M., Sipahi, F., Temizel, İ., Çakmak, G., Güloglu, Z. S. 2018. Petrography, mineral chemistry and crystallization conditions of Cenozoic plutonic rocks located to the north of Bayburt (Eastern Pontides, Turkey). Bullettin of the Mineral Research and Exploration 157, 75–102.

Kaygusuz, A., Yücel, C., Arslan, M., Temizel, İ., Yi, K., Jeong, Y. J., Siebel, W., Sipahi, F. 2020. Eocene I-type magmatism in the Eastern Pontides, NE Turkey: insights into magma genesis and magma-tectonic evolution from whole-rock geochemistry, geochronology and isotope systematics. International Geology Review 62, 1406–1432.

Kaygusuz, A., Arslan, M., Temizel, İ., Yücel, C., Aydınçakır, E. 2021. U–Pb zircon ages and petrogenesis of the

Late Cretaceous I-type granitoids in arc setting, Eastern Pontides, NE Turkey. Journal of African Earth Sciences 174, 104040.

Kaygusuz, A., Yücel, C., Aydınçakır, E., Gücer, M. A., Ruffet, G. 2022. 40Ar–39Ar dating, whole-rock and Sr-Nd isotope geochemistry of the Middle Eocene calc-alkaline volcanic rocks in the Bayburt area, Eastern Pontides (NE Turkey): Implications for magma evolution in an extension-related setting. Mineralogy and Petrology 116, 379–399.

Kaygusuz, A., Güloğlu, Z. S., Aydınçakır, E., Yücel, C., Vural, A., Siebel, W., Jeong, Y-J. 2023. U–Pb zircon dating, Sr-Nd whole-rock and Lu-Hf zircon isotope analyses of the Eocene Arslandede pluton, Eastern Pontides, NE Turkey: Implications for mantle source and magma evolution. Chemie der Erde- Geochemistry.

Kemp, A. I. S. 2001. Petrogenesis of granitic rocks: A source-based perspective. PhD Thesis, Autralian National University, Canberra, Australia (unpublished).

Kemp, A. I. S. 2004. Petrology of high-Mg, low-Ti igneous rocks of the Glenelg River Complex (SE Australia) and the nature of their interaction with crustal melts, Lithos, 78, 119-156.

Leake, E. B., Wooley, A. R., Arps, C. E. S., Birch, W. D., Gilbert, M. C., Grice, J. D., Hawthorne, F. C., Kato, A., Kisch, H. J., Krivovichev, V. G., Linthout, K., Laird, J., Mandarino, J., Maresch, W. V., Nickhel, E. H., Rock, N. M. S., Schumacher, J. C., Smith, D. C., Stephenson, N. C. N., Ungaretti, L., Whittaker, E. J. W., Youzhi, G. 1997. Nomenclature of amphiboles report of the subcommittee on amphiboles of the international mineralogical association commission on new minerals and mineral names. European Journal Mineralogy, 9, 623-651.

Liu, Z., Zhu, D. C., Wang, Q., Eyüboğlu, Y., Zhao, Z. D., Liu, S. A., Xu, L. J. 2018. Transition from low-K to high-K calc-alkaline magmatism at approximately 84 Ma in the Eastern Pontides (NE Turkey): Magmatic response to slab rollback of the Black Sea. Journal of Geophysical Research Solid Earth 123, 7604–7628.

Luhr, J. F., Carmichael, I. S. E., Varekamp, J. C. 1984. The 1982 eruptions of El Chicón Volcano, Chiapas, Mexico: Mineralogy and petrology of the anhydrite-bearing pumices: Journal of Volcanology and Geothermal Research 23, 69-108.

Merzbacher, C., Eggler, D. H. 1984. A magmatic geohygrometer: Application to Mount St. Helens and other dacitic magmas, Geology 12, 587-590.

Moazzen, M., Droop, G. T. R. 2004. Application of mineral thermometers and barometers to granitoid igneous rocks: The etive complex, W Scotland. Mineralogy and Petrology 83, 27-53.

Naney, M. T. 1983. Phase equilibria of rock-forming ferromagnesian silicates in granitic systems, American Journal of Science 283, 993-1033.

Nielsen, C. H., Sigurdsson, H. 1981. Quantitative methods for electron microprobe analysis of sodium in natural and synthetic glasses. American Mineralogist 66(5-6), 547-552.

Nixon, G. T. 1988. Petrology of the younger andesites and dacites of Iztaaccihuatl volcano, Mexico: Disequilibrium phenocryst assemblages as indicators of magma chamber processes. Journal of Petrology 29, 213-264.

Oğuz-Saka, S., Aydin, F., Karsli, O., Dokuz, A., Aiglsperger, T., Miggins, D. P., Şen, C., Kandemir, R., Sarı, B., Koppers, A. A. P. 2023. Two-stage bimodal volcanism in a Late Cretaceous arc/back-arc setting, NE Turkey: Constraints from volcano-stratigraphy, zircon U-Pb and $^{40}Ar/^{39}Ar$ geochronology and whole-rock elemental and Sr-Nd-Pb isotope geochemistry. Lithos.

Okay, A., Şahintürk, Ö. 1997. Geology of the eastern Pontides. In: Robinson AG (Ed.) Regional and petroleum geology of the Black Sea and surrounding region. American Association of Petroleum Geologists Memoirs 68, 291–311.

Özdamar, Ş. 2016. Geochemistry and geochronology of late Mesozoic volcanic rocks in the northern part of the Eastern Pontide Orogenic Belt (NE Turkey): implications for the closure of the Neo-Tethys Ocean. Lithos 248–251, 240–256.

Özdamar, Ş., Roden, M. F., Billor, M. Z. 2017. Petrology of the shoshonitic Çambaşı pluton in NE Turkey and implications for the closure of the Neo-Tethys Ocean: Insights from geochemistry, geochronology and Sr–Nd isotopes. Lithos 284–285, 477–492.

Parsons, I., Mason, R. A., Becker, S. M., Finch, A. A. 1991. Biotite equilibria and fluid circulation in the Klokken Intrusion. Journal of Petrology 32, 1299-1333.

Perugini, D., Busa, T., Poli, G., Nazzareni, S. 2003. The role of chaotic dynamics and flow fields in the development of disequilibrium textures in volcanic rock. Journal of Petrology 44, 733-756.

Revan, M. K., Demir, Y., Uysal, İ., Özkan, M., Dumanlılar, Ö., Şen, C., Kara, R. T., Hamzaçebi, S., Göç, D., Müller, D., Tokoğlu, M. 2023. Recently-discovered Bahçecik Au±Ag mineralization in the Eastern Pontides, Gümüşhane-NE Türkiye: geological and geochemical implications on the intermediate sulfidation epithermal deposit. Internatıonal Geology Review.

Rezeau, H., Hässig, M., Sadikhov, E., Chiaradia, M., Moritz, R. 2023. Magmatic record along the Eastern Pontides-Lesser Caucasus orogenic belt: Implications for magma petrogenesis, regional tectonics and metallogeny. Earth-Science Reviews.

Ridolfi, F., Renzulli, A. 2012. Calcic amphiboles in calc-alkaline and alkaline magmas: Thermobarometric and chemometric empirical equations valid up to 1,130 °C and 2.2 Gpa. Contributions to Mineralogy and Petrology 163, 877-895.

Ridolfi, F., Renzulli, A., Puerini, M. 2010. Stability and chemical equilibrium of amphibole in calc-alkaline magmas: An overview, new thermobarometric formulations and application to subduction-related volcanos, Contributions to Mineralogy and Petrology 160, 45-66.

Rutherford, M. J., Hill, P. M. 1993. Magma ascent rates from amphibole breakdown: an experimental study applied to the 1980-1986 Mount St. Helens eruptions. Journal of Geophysical Research 98, 19667-19685.

Sakumaya, M. 1981. Petrological study of the Myoko and Kurohime Volcanoes, Japan: crystallization sequence and evidence magma mixing. Journal of Petrology 22, 553-583.

Sar, A., Kürüm, S., Bingöl, A. F. 2023. Early Cretaceous to Middle Eocene magmatic evolution of Eastern Pontides: Zircon U-Pb ages and Hf isotopes, and geochemical and Sr-Nd isotopic constraints from multiphase granitoids, NE Turkey. Journal of Earth Science 34, 2, 518-535.

Schmidt, M. W. 1992. Amphibole composition in tonalite as a function of pressure: An experimental calibration of the Al-in-hornblende barometer, Contributions to Mineralogy and Petrology 110, 304-310.

Simonetti, A., Shore, M., Bell, K. 1996. Diopside phenocrysts from nephelinite lavas, Napak Volcano, Eastern Uganda: Evidence from magma mixing. Canadian Mineralogist 34, 411-442.

Sipahi, F., Akpınar, İ., Saydam Eker, Ç., Kaygusuz, A**.,** Vural, A**.**, Yılmaz, M. 2017. Formation of the Eğrikar (Gümüşhane) Fe–Cu skarn type mineralization in NE Turkey: U–Pb zircon age, lithogeochemistry, mineral chemistry, fluid inclusion, and O-H-C-S isotopic compositions. Journal of Geochemical Exploration 182, 32–52.

Smith, J. V., Brown, W. L. 1988. Feldspar minerals I: Crystal structures, physical, chemical, and microtextural properties, Springer Verlage, New York.

Speer, J. A. 1984. Micas in igneous rocks, Micas, Reviews in Mineralogy, ed: Bailey S.W, 13, 299-35.

Stimac, J. A., Pearce, T. H. 1992. Textural evidence of mafic-felsic magma interaction in dacite lavas, Clear Lake, California. American Mineralogist 77, 795-809.

Streck, M. J. 2008. Mineral textures and zoning as evidence for open system processes. In: Putirka KD, Tepley III FJ (eds) Minerals, inclusions and volcanic processes. Miner. Soc. Am and Geochemical Soc, Rev Minaral 595-622.

Streckeisen, A. 1976. To each plutonic rock its proper name. Earth Science Reviews 12, 1–33.

Temizel, İ., Arslan, M., Ruffet, G., Peucat, J.J. 2012. Petrochemistry, geochronology and Sr-Nd isotopic systematics of the Tertiary collisional and post-collisional volcanic rocks from the Ulubey (Ordu) area, eastern Pontide, NE Turkey: implications for extension-related origin and mantle source characteristics. Lithos 128, 126–147

Temizel, İ., Abdioğlu Yazar, E., Arslan, M., Kaygusuz, A., Aslan, Z. 2018. Mineral chemistry, whole-rock geochemistry and petrology of Eocene I-type shoshonitic plutons in the Gölköy area (Ordu, NE Turkey). Bullettin of the Mineral Research and Exploration 157, 121–152.

Temizel, İ., Arslan, M., Yücel, C., Abdioğlu Yazar, E., Kaygusuz, A., Aslan, Z. 2019. U-Pb geochronology, bulk-rock geochemistry and petrology of Late Cretaceous syenitic plutons in the Gölköy (Ordu) area (NE Turkey): Implications for magma generation in a continental arc extension triggered by slab roll-back. Journal Asian Earth Sciences 171, 305–320.

Temizel, İ., Arslan, M., Yücel, C., Abdioğlu Yazar, E., Kaygusuz, A., Aslan, Z. 2020. Eocene tonalite–granodiorite from the Havza (Samsun) area, northern Turkey: adakite-like melts of lithospheric mantle and crust generated in a post-collisional setting. International Geology Review 62, 1131–1158.

Temizel, İ., Arslan, M., Abdioğlu Yazar, E., Aslan, Z., Kaygusuz, A., Baki Eraydın, T. 2022. Zircon U-Pb geochronology and petrology of the tholeiitic gabbro from the Kovanlık (Giresun) area: Constraints for the Late Cretaceous bimodal arc magmatism in the Eastern Pontides Orogenic Belt, NE Turkey. Lithos 428–429. Toksoy-Köksal, F. 2016. Ekecidağ Magmatik Birliği (Orta Anadolu) Granitoyidlerinin Petrojenezi: Mineral Kimyası Perspektifi. Yerbilimleri 37(2), 139-178.

Topuz, G., Altherr, R., Schwarz, W. H., Siebel, W., Satır, M., Dokuz, A. 2005. Post-collisional plutonism with adakite-like signatures: The Eocene Saraycik granodiorite (Eastern Pontides, Turkey). Contributions to Mineralogy and Petrology 150, 441–455.

Topuz, G., Altherr, R., Siebel, W., Schwarz, W.H., Zack, T., Hasözbek, A., Barth, M., Satir, M., Şen, C. 2010. Carboniferous high-potassium I-type granitoid magmatism in the Eastern Pontides: The Gümüşhane pluton (NE Turkey). Lithos 116, 92–110.

Topuz, G., Okay, A. I., Altherr, R., Schwarz, W. H., Siebel, W., Zack, T., Satir, M., Sen, C. 2011. Post-collisional adakite-like magmatism in the Agvanis Massif and implications for the evolution of the Eocene magmatism in the Eastern Pontides (NE Turkey). Lithos 125, 131–150.

Tulloch, A. J., Challis, G. A. 2000. Emplacement depths of Palaeozoic-Mesozoic plutons from western New Zealand estimated by hornblend-Al geobarometry. New Zealand Journal of Geology and Geophysics 43, 555-567.

Uchida, E., Endo, S., Makino, M. 2007. Relationship between solidification depth of granitic rocks and formation of hydrothermal ore deposits: Resource Geology 57, 47-56.

Ustaömer, T., Robertson, A. H. F., Ustaömer, P. A., Gerdes, A., Peytcheva, I. 2013. Constraints on Variscan and Cimmerian magmatism and metamorphism in the Pontides (Yusufeli-Artvin area), NE Turkey from U-Pb dating and granite geochemistry. Geological Society Special Publication 372, 49–74.

Venezky, D. Y., Rutherford, M. J. 1997. Preeruption conditions and timing of dacite-andesite magma mixing in the 2.2 ka eruption at Mount Rainier. Journal Geophys Res. 102, 20069-20086.

Vural, A., Kaygusuz, A. 2021. Geochronology, petrogenesis and tectonic importance of Eocene I-type magmatism in the Eastern Pontides, NE Turkey. Arabian Journal of Geosciences 14. https://doi.org/10.1007/s12517-021-06884-z.

Wallace, P. J., Carmichael, I. S. E. 1994. Petrology of Volcan Tequila, Jalisco, Mexico: Disequilibrium phenocryst assemblages and evolution of the subvolcanic magma system. Contributions to Mineralogy and Petrology 117, 345-361.

Wones, D. R. 1989. Significance of the assemblage titanite, magnetite, quartz in granitic rocks. American Mineralogist 74, 744-749.

Yılmaz, Y. 1972. Petrology and structure of the Gümüşhane Granite and surrounding rocks, North-Eastern Anatolia. PhD Thesis, Univ. London 260 p.

Yücel, C., Arslan, M., Temizel, İ., Abdioğlu Yazar, E., Ruffet, G. 2017. Evolution of K-rich magmas derived from a net veined lithospheric mantle in an ongoing extensional setting: Geochronology and geochemistry of Eocene and Miocene volcanic rocks from Eastern Pontides (Turkey). Gondwana Research 45, 65–86.

Yücel, C., Aydınçakır, E., Kaygusuz, A., Arslan, M., Yi, K., Jeong, Y-J., Cicerali, D. 2023. Petrogenesis of Late Cretaceous A-type plutonic rocks from the Eastern Pontides Orogenic Belt (NE Turkey): Constraints from zircon U-Pb geochronology, zircon Lu-Hf and whole-rock Sr-Nd-Pb-Hf isotopes. International Geology Review.